Scatterer Density in Edge and Coherence Enhancing Nonlinear Anisotropic Diffusion for Medical Ultrasound Speckle Reduction

Ahmed Badawi, J. Michael Johnson, and Mohamed Mahfouz

Abstract—This paper proposes new enhancement models to the methods of nonlinear anisotropic diffusion to greatly reduce speckle and preserve image features in medical ultrasound images. By incorporating local physical characteristics of the image, in this case scatterer density, in addition to the gradient, into existing tensor-based image diffusion methods, we were able to greatly improve the performance of the existing filtering methods, namely edge enhancing (EE) and coherence enhancing (CE) diffusion. The new enhancement methods were tested using various ultrasound images, including phantom and some clinical images, to determine the amount of speckle reduction, edge, and coherence enhancements. Scatterer density weighted nonlinear anisotropic diffusion (SDWNAD) for ultrasound images consistently outperformed its traditional tensor-based counterparts that use gradient only to weight the diffusivity function. SDWNAD is shown to greatly reduce speckle noise while preserving image features as edges, orientation coherence, and scatterer density. SDWNAD superior performances over nonlinear coherent diffusion (NCD), speckle reducing anisotropic diffusion (SRAD), adaptive weighted median filter (AWMF), wavelet shrinkage (WS), and wavelet shrinkage with contrast enhancement (WSCE), make these methods ideal preprocessing steps for automatic segmentation in ultrasound imaging.

Keywords—Nonlinear anisotropic diffusion, ultrasound imaging, speckle reduction, scatterer density estimation, edge based enhancement, coherence enhancement.

I. INTRODUCTION

MEDICAL ultrasound imaging is an important imaging modality for diagnostic procedures [1]. There are three primary characteristics that contribute to the widespread use of medical ultrasound. Ultrasound is a real-time modality, does not utilize ionizing radiation, and provides quantitative measurement and imaging of blood flow. However,

Ahmed Badawi is a visiting professor with University of Tennessee, Knoxville, Biomedical Engineering Department and professor on leave at Systems and Biomedical Engineering, Cairo University. Address: 315 Perkins Hall, Knoxville, TN, 37996, USA. Phone: 865-974-6009; Fax: 865-946-1787; (email: ambadawi@utk.edu).

J. Michael Johnson is a PhD student at Biomedical Engineering Department, University of Tennessee, Knoxville (email: jjohn138@cmr.utk.edu).

Mohamed Mahfouz is associate professor with University of Tennessee, Knoxville, Biomedical Engineering Department, 301 Perkins Hall (email: mmahfouz@utk.edu).

ultrasound does have one major shortcoming – the presence of speckle noise. Speckle is a random interference pattern present in all images obtained using coherent radiation in a medium containing subresolution scatterers. Speckle has a negative impact on ultrasounds images because the speckle pattern does not correspond to the underlying structure of the image. Work by Bamber and Daft suggest that speckle may reduce the detectability of a lesion by approximately a factor of eight [2]. Speckle is ultimately responsible for the poorer effective resolution of medical ultrasound when compared to other medical modalities. Therefore, speckle reduction has become an active area of research [3].

Several methods of speckle reduction have been proposed [6,9-15,21-26]. Bamber et al. studied adaptive filtering for speckle reduction which changes the amount of smoothing depending on the ratio of local variance to local mean [6]. In order to preserve details, Bamber et al. smoothing is increased in homogenous regions while reduced or totally avoided in other regions. Bamber et al. method has a difficulty to removing speckle near or on image edges. The adaptive weighted median filter (AWMF) [38] is based on the pixel replication method used in traditional median filter but it has the assumption that speckle must be smaller than half of the filter window size making it sensitive to some empirically determined parameters. Abd–Elmoniem et al. [13] presented a tensor-based anisotropic diffusion method, a nonlinear coherent diffusion (NCD) for speckle reduction and coherence enhancement [12-13]. Wavelet shrinkage (WS), and wavelet shrinkage with contrast enhancement (WSCE) methods are referred in [13] as a wavelet speckle reduction methods.

A speckle reduction and structure enhancement method by multichannel median boosted anisotropic diffusion was presented in [39] and showed to be superior to methods like AWFM and Gaussian regularized anisotropic diffusion. While NCD had a better performance compared to AWFM, WS, and WSCE, it has several criticisms mentioned in [39]. One such criticism being anisotropic tensor formulation is regarding the size of speckle that may occupy more than the size of a pixel.

Lee [22], Frost [23], and Kuan [24-25] proposed noise reduction filters based on the multiplicative speckle model. Yu and Acton [26] developed a speckle reducing anisotropic diffusion (SRAD) filtering scheme based upon work by Lee and Frost. Their SRAD filter developed to suppress speckles while preserving edges has shown good performance as NCD with different levels of speckle. NCD and SRAD can preserve and enhance prominent edges when removing speckle, but

World Academy of Science, Engineering and Technology
International Journal of Medical and Health Sciences
Vol:1, No:5, 2007

they have common limitation in retaining subtle features as small cysts or lesions in ultrasound images. While the multichannel median boosted anisotropic diffusion method presented in [39] was successful compared to AWFM and Gaussian regularized anisotropic diffusion, their results with test ultrasound phantoms and clinical ultrasound images of different levels of speckle noise, size, and distribution were not compared.

Ideally, though, denoising techniques should not only reduce noise, but also prevent blurring and preserve signal edges. Since the work of Perona and Malek in 1987 [7], the use of partial differential equations has been studied as a way of increasing the inhomogeneity of denoising filters. This is ideal because a constant (in space and time) diffusivity equation gives rise to a linear diffusion equation with the undesirable characteristics of homogeneous diffusion, which smoothes the entire image, including edges. By introducing an inhomogeneous diffusivity equation, which depends upon x, y, and the image being filtered, one can create filters which prevent edge blurring while reducing noise. Perona and Malek implemented this filtering technique by introducing a function based on the derivative of the image at time t [8]. This isotropic (the diffusivity function is a scalar) case of inhomogeneous diffusion does a fairly decent edges preservation, while smoothing background noise.

Diffusion-based denoising is affected by several factors such as the choice of diffusivity function, the method used for discretization of the PDE, the choice of parameters used for solving the PDE including the diffusivity constant, and the method used for solving the system of equations. Quite often the edges are noisy, causing inaccurate edge preservation or edge smoothing when the isotropic filter is used [17]. Therefore, Weickert proposed two tensor based filtering methods which attempt incorporate the directionality in the image to better estimate the perceptual orientation of the edges and thus these diffusion methods have increased feature preservation characteristics as compared to isotropic diffusion [35-36]. The first such filtering method, introduced as 'edge enhancing diffusion', involves constructing the diffusion tensor so that it mirrors the edge structure, thus preserving the edges by smoothing parallel to the edges. This allows smoothing near the edge, while preserving the edges themselves. Later, Weickert introduced coherence enhancing diffusion [36]. The diffusion tensor is built using the well known structure tensor [36], so that the filter incorporates the coherence of the image to better preserve the flow-like features in the image. Both methods have been shown to be more effective at preserving image features than the isotropic case. Again, the performance of these techniques is subject to choices, such as the stencil used for solving the nonlinear tensor diffusion equation and the various parameters in the diffusivity functions.

Mean square error and signal to noise ratio are often used for tuning and evaluating the denoising process [13, 16-17]. Signal-to-noise ratio (SNR) and Peak signal-to-noise-ratio (PSNR) image measures are derived from the root mean squared error (RMSE) and used as image quality measures in compression, representation, and standards [19, 31]. Higher quality measures do not always mean better visual quality of enhanced edges and denoised structures. Edge enhancement

and edge preserving quantitative evaluation is applied by the Pratt's figure of merit (FOM) as a measure for edge preservation and edge enhancement between the ideal image and processed one, and can be used as a measure of an object's segmentation quality [34].

Incorporating the scatterer density in the image into the nonlinear isotropic diffusivity equations was proposed in [27]. This method demonstrated improved performance over previous methods, which use gradient alone to weight diffusivity function. Our paper proposes a new method for tensor based diffusion to reduce speckle in ultrasound images. We propose including the scatterer density in the formulation of the anisotropic diffusion tensor, allowing further improvement of the edge and orientation preserving characteristics of nonlinear anisotropic diffusion. For reasons of computational simplicity, the case of tensor-based diffusion was implemented using the standard stencil described by Weickert in [37].

II. NON LINEAR DIFFUSION

A. Nonlinear Diffusion in Image Denoising

Diffusion is a physical process describing the equilibration of two unequal concentrations without creating or destroying mass. In mathematical terms, if u is the concentration and C is the diffusivity function, then the diffusion equation can be written as:

$$\partial_t u = div(C\nabla u) \tag{1}$$

When dealing with images, the analog of the concentration, u, is the grey scale intensity level. When C is constant, we describe the diffusion as *homogeneous*. When C varies with position x, y, we describe the diffusion as *inhomogeneous*. Often the diffusivity function is a function of the local gradient at time t or some other image feature, therefore the diffusion filter is said to be a *nonlinear*. The diffusion-based filter calculates a filtered image $u(x,y,t)$ of the original noisy image $f(x,y)$ as a solution to the nonlinear diffusion equation as shown:

$$\partial_t u = div(C(x,y)\nabla u) \tag{2}$$

with the original image $f(x,y)$ as the initial state:

$$u(x,y,0) = f(x,y), \tag{3}$$

and reflecting boundary conditions on the image boundary:

$$\partial_n u := 0 \tag{4}$$

where n denotes the normal to the image boundary. The nonlinear diffusivity function $C(x,y)$ is usually given as a strictly decreasing function of the magnitude of the gradient.

Perona and Malek suggested including the image gradient in the definition of the diffusivity function to produce adaptive edge preserving diffusion filters [8]. Since then, several authors have suggested different diffusivity functions based on the image gradient, some are shown in [17]. However, incorporating other physical image characteristics has, until recently received little attention.

Previous work has shown that weighting the gradient by the scatterer density in the diffusion equation (Isotropic case) increases the noise reduction and edge enhancing performance of the filter [27]. In this paper we attempt to incorporate those

World Academy of Science, Engineering and Technology
International Journal of Medical and Health Sciences
Vol:1, No:5, 2007

same image characteristics for the anisotropic tensor formulated case to study filters performance on the edge and coherence orientation preserving characteristics of these filters.

B. Image Gradient

Gradient edge detection is the most widely used technique to weight the nonlinear diffusion filters. To calculate the gradient, the image *f(x,y)* is convolved with two kernels. One estimates the gradient in the horizontal direction, G_x, and one estimates the gradient in the vertical direction, G_y. The magnitude of the gradient for any point *f(x,y)* can be written as:

$$|\nabla f| = \sqrt{G_x^2 + G_y^2} \, , \qquad (5)$$

III. ULTRASOUND SCATTERER DENSITY MODEL

Previously it has been shown that NLD methods can be improved by including the scatterer density in the diffusivity equation. Scatter density has been shown to increase in areas of large scatteres density and wherever there is a transition between different tissue mediums. Therefore, the scatterer density gives a meaningful measurement of the physical characteristics of the image.

For a large number of scatterers (infinite), the Rayleigh distribution can be used to model the scatterer density. However, in most cases the scatterer density is finite [13]. Therefore, a model to determine the distribution of a finite number of 'effective' scatterers is needed. The proposed solution to the problem utilizes the so-called K distribution [4,18]. The envelope of the received backscatterered signal, *A*, can be evaluated as:

$$p(A) = 2\left(\frac{A}{2}\right)^\alpha \frac{b^{\alpha+1}}{\Gamma(\alpha)} K_{\alpha-1}(bA) \, , \qquad (6)$$

where $b = \sqrt{\frac{4\alpha}{E\{A^2\}}}$ and $K_\beta()$ is the modified Bessel function of the second kind of order β. The K distribution is a generalization of the Rayleigh distribution, allowing one to account for a finite number of 'effective' scatterers, which is represented by the term α in Eq. (6). To solve for the effective number of scatterers, α, we use the K distribution moments [4,18], which can be written in closed form as:

$$E\{A^\eta\} = \frac{(2\sigma^2)^{\eta/2}\Gamma(1+\eta/2)\Gamma(\alpha+\eta/2)}{\alpha^{\eta/2}\Gamma(\alpha)} \, , \qquad (7)$$

Writing the expression for the moments in closed form allows one to estimate the parameters of the K-distributed data using sample moments. Blacknell [5] used normalized moments to estimate the scatterer density, α. In this work we use the method of second and fourth order moments to estimate α. Using Eq. (7), the normalized ratio of the fourth moment to the second moment squared can be written as:

$$\frac{E\{A^4\}}{E^2\{A^2\}} = 2(1 + \frac{1}{\alpha}) \, , \qquad (8)$$

Replacing $E\{A^4\}$ and $E^2\{A^2\}$ with the corresponding sample moments, and solving for α, we obtain and estimate for the scatterer density, $\hat{\alpha}$:

$$\hat{\alpha} = \frac{2}{\frac{\mu_4}{\mu_2^2} - 2} \, , \qquad (9)$$

where the sample moments are given by:

$$\mu_\nu = \frac{1}{N}\sum_{i=1}^{N} A_i^\nu \, , \qquad (10)$$

where the A_i are the *N* samples of the envelope of the received backscattered signal used to estimate the parameters of the K distributed data from fourth order moment, μ_4, and second order moment, μ_2 for a window of size H x W. μ_2 and μ_4 can be directly calculated from the window histogram. Previous estimates of the scatterer density parameter have used large window sizes (33 x 32) for characterization of reperfused infracted myocardium from high frequency intracardiac ultrasound imaging [28-29]. This research resulted in values of α ranging from 2 to 15. It also showed the physical meaningfulness of the scatterer density parameter, which displayed a significant ability to help characterize normal from infracted myocardium. In our research we calculated *α* using a 7x3 window to emulate the effective resolution in the image. In scatterer density weighted nonlinear diffusion (SDWND) filters presented here, we propose two methods of incorporating the scatterer density into the diffusion equation. We weighted the gradient factor by the scatterer density in both edge enhancing diffusion (SDWNEED) and coherence enhancing diffusion (SDWNCED).

IV. FLOW OF THE DENOISING PROCESS

The diffusion equation, in general, can be written as:

$$\frac{\partial}{\partial t}U(x,y,t) = \nabla \bullet (C(x,y,t)\nabla U(x,y,t)) \, , \qquad (11)$$

where "•" represents the inner product of two vectors. When *C* is a scalar function, the diffusion process is isotropic. When *C* is a tensor-based function of the directional parameters, the process becomes anisotropic. To solve the above PDE, the original image u_o is used as the initial condition and the Neumann boundary condition is applied to the image borders:

$$u(x,y,t)_{t=0} = u_o = f(x,y) \, , \quad \partial_n u = 0. \qquad (12)$$

The Neumann boundary condition avoids the energy loss in the image boundary during the evolution of the diffusion process. Several different diffusivity functions, *C(x,y,t)*, exist in the literature [17]. The most common are:

Perona-Malik 1: $C(x,y,t) = 1/(1 + \frac{|\nabla U_\sigma|^2}{K^2})$ $\qquad (13)$

Perona-Malik 2: $C(x,y,t) = \exp(-|\nabla U_\sigma|^2 / 2K^2)$ $\qquad (14)$

Charbonnier: $C(x,y,t) = \left(1 + \frac{|\nabla U_\sigma|^2}{K^2}\right)^{-1/2}$ $\qquad (15)$

Weickert (with m=2, 3, and 4): $\qquad (16)$

World Academy of Science, Engineering and Technology
International Journal of Medical and Health Sciences
Vol:1, No:5, 2007

$$C(x,y,t) = \begin{cases} 1 & If\ |\nabla U_\sigma| = 0 \\ 1 - \exp(-\dfrac{C_m}{(|\nabla U_\sigma|^2 / K^2)^m}) & If\ |\nabla U_\sigma| > 0 \end{cases}$$

$$1 = \exp(-C_m)(1 + 2C_m m) \tag{17}$$

for m=2, 3, and 4, C_m=2.33666, 2.9183, and 3.31488. In Eqs. (13)-(16), U_σ represents the regularization of the image, U. This step is necessary because the original formulation of the problem by Perona and Malek was ill-posed [16], where similar images would produce very different solutions. The common solution is to preprocess, or regularize, the image by convolving it with a Gaussian kernel of standard deviation σ so that U_σ can be written as:

$$\nabla U_\sigma = \nabla(G_\sigma * U(x,y,t)) \tag{18}$$

A. Edge Enhancing Diffusion

In tensor based diffusion, the PDE for the anisotropic case is given as [35,17]:

$$\partial_t u = \nabla \bullet (D \nabla u) \tag{19}$$

where D is a positive semi-definite symmetric diffusion tensor. The 2x2 matrix, D, can be written in terms of its eigenvectors, $\mathbf{v_1}$ and $\mathbf{v_2}$, and eigenvalues, λ_1 and λ_2:

$$D = \begin{bmatrix} \vec{v}_1 & \vec{v}_2 \end{bmatrix} \begin{bmatrix} \lambda_1 & 0 \\ 0 & \lambda_2 \end{bmatrix} \begin{bmatrix} \vec{v}_1^T \\ \vec{v}_2^T \end{bmatrix} \tag{20}$$

For the case of edge enhancing diffusion (EE) the eigenvectors are defined as follows:

$$\vec{v}_1 \| \nabla u_\sigma \quad and \quad \vec{v}_2 \perp \nabla u_\sigma \tag{21}$$

where u_σ is the normalized, or smoothed version of the image. This is defined as the image convolved with a Guassian kernel with standard deviation σ. Often, $\lambda_2 = 1$, which allows smoothing in the $\mathbf{v_2}$ direction. Then λ_1 is taken to be $C(x,y,t)$ as defined in Eqs. (13)-(16).

In EE diffusion, we examine two methods of edge enhancing diffusion. In the first, $\lambda_2 = 1$ and $\lambda_1 = C(x,y,t)$. In the second case we define $\lambda_1 = C(x,y,t)$, and the second eigenvalue as:

$$\lambda_2 = \frac{1}{Kv} * C(x,y,t) \tag{22}$$

Where K_v is a constant ≥ 1, and is set in our experiment to 5.

B. Coherence Enhancing Diffusion

In coherence enhancing (CE) diffusion, the diffusion tensor is given as [36]:

$$D = \begin{bmatrix} a & b \\ b & c \end{bmatrix} = R^T \begin{bmatrix} c_1 & 0 \\ 0 & c_2 \end{bmatrix} R \tag{23}$$

Where R is the rotation matrix, whose columns are the eigenvectors of the structure tensor S, which is defined as:

$$S = \begin{bmatrix} s_{11} & s_{12} \\ s_{12} & s_{22} \end{bmatrix} = \begin{bmatrix} u_x u_x * G_\sigma & u_x u_y * G_\sigma \\ u_x u_y * G_\sigma & u_y u_y * G_\sigma \end{bmatrix} \tag{24}$$

where $* G_\sigma$ represents the convolution with a Gaussian kernel of standard deviation σ. In our work we define c_1 and c_2 for each pixel as:

$$c_2 = C(x,y,t) = C(|\nabla u|) \tag{25}$$

$$c_1 = \max(c_2, 1 - \exp(-(\lambda_1 - \lambda_2)^2 / k^2)) \tag{26}$$

where k is small constant ($0 < k < 1$). The eigenvalues of the structure tensor, λ_1 and λ_2, are defined as:

$$\lambda_{1,2} = \frac{1}{2}(s_{11} + s_{22} \pm \delta) \tag{27}$$

$$\delta = \sqrt{((s_{11} - s_{22})^2 + 4 \cdot s_{12}^2)} \tag{28}$$

Solving for the components of the diffusion tensor:

$$a = \frac{1}{2}\left(c_1 + c_2 + \frac{((c_2 - c_1)(s_{11} - s_{22}))}{\delta}\right) \tag{29}$$

$$b = \frac{((c_2 - c_1)s_{12})}{\delta} \tag{30}$$

$$c = \frac{1}{2}\left(c_1 + c_2 - \frac{((c_2 - c_1)(s_{11} - s_{22}))}{\delta}\right) \tag{31}$$

In this paper we will compare the proposed CED filter described in Eqs. (23) - (31) after incorporating scatterer density into diffusivity function with a more traditional filter described in [33]. It is identical to the proposed method except for that, in the latter case, c_2 is a small ($0 < c_2 < 1$) constant.

V. SOLTION TO THE DIFFUSION EQUATION

The straight forward solution to the diffusion equation is obtained using finite differences [33, 36-37]. By replacing spatial derivatives with central differences and $\partial u / \partial t$ with a forward difference approximation, we can solve for a future numerical value of u using only values from the previous time step without complex systems of equations. This is the so-called explicit scheme which can be represented as:

$$\frac{u_{i,j}^{k+1} - u_{i,j}^k}{\tau} = A_{i,j}^k * u_{i,j}^k \tag{32}$$

where the time, T, is given as $k\tau$ at iteration k with time step size τ and $u_{i,j}^k$ is the approximation of $u(x,y,t)$ at pixel (i, j). $A_{i,j}^k * u_{i,j}^k$ is the discretization of the right-hand side of the diffusion equation, where $A_{i,j}^k$ is a 3x3 stencil that varies in time and space which is convolved with the image at iteration k. The discretization for the stencil used in this work (Fig. 1) is provided by Weickert in [37].

The standard stencil in [37] was used in this work for computational ease, however it is not stable for larger τ values. A more complex stencil has been presented which allows the use of larger values of τ, approximately ten times greater than the allowed with the standard discretization [37, 13]. Since our main aim of this study was to investigate the scatterer density into the nonlinear diffusion equation and study how better it enhances the quality and preservation of all image features including scatterer density, we used the straightforward discretization scheme [37] regardless of its being unstable for large values of τ.

VI. PROPOSED METHODS

It is known that connective tissue with varying amounts of collagen and elastic fibers is a major source of scattering in

World Academy of Science, Engineering and Technology
International Journal of Medical and Health Sciences
Vol:1, No:5, 2007

Ultrasound images. It is also known that collagen density in liver parenchyma determine how elastic the liver tissue is. In cases of liver cirrhosis, an increase in the amount of collagen causes a rigidity of the tissues with palpation and thus presents an increase in the ultrasound image brightness. Blood vessels contain varying amounts of collagen and elastic fibers which controls the supportive and elastic pattern of the vessels depending on size and function of these vessels. The blood vessels containing these fibers are major ultrasound scattering sources which in addition to the reflection between their interfaces show a contrast in imaging between the vessel walls and the blood. Scatterer density varies in tissues and vessels depending on the ratio of these fibers to the other histological contents. Scatterer density is higher in anatomy near tissue edges and blood vessels. In section III, as there is an estimate of this scatterer density per resolution cell (α), we have proposed in [27] to incorporate this physical and tissue parameter to weight the diffusivity function. Researchers [28-30] rely on the estimation of this physical parameter to characterize tissues and abnormalities. In the following sections, we show how to incorporate this physical parameter into the diffusion equation. Thus anisotropy in the diffusion equation will not only be in the gradient describing edges, coherency in orientation and geometry of structure but also be in the scatterer density distribution in local regions. We will show how this important physical parameter enhances the images and produces an image with the diffusion evolution that anatomically corresponds to the geometrical underlying structure with speckle reduction, edge preservation, and coherence enhancement.

A. Proposed Diffusivity Function

We propose applying the modified diffusivity function given in [27]:

$$C(x,y,t) = C(\alpha|\nabla u|) \tag{33}$$

where α is the scatterer density estimate. Now any of the previously mentioned diffusivity functions can be weighted by α and the gradient. Taking (13) as an example:

$$C(x,y,t) = C(\alpha|\nabla u|) = 1/\left(1 + \frac{(\alpha|\nabla u|)^2}{K^2}\right) \tag{34}$$

The scatterer density is measured locally using a H x W window. The function $C(x,y,t)$ can be any of the existing diffusion functions in the literature and is calculated at each time, t, of the diffusion process. For edge enhancing diffusion (EED) the modified equation is to let $\lambda_2 = 1$ and change λ_1 to be $C(\alpha|\nabla u|)$. For coherence enhancing diffusion (CED), we let c_1 in Eq. (26), and calculating the value of c_2 using the scatterer density weighted diffusion equation (Eq. (34)). In (26,34) the c_2 is a function of edge and scatterer density content, so depending on the dominant parameter, c_2 will be determined. c_1 is a function of edge, orientation coherency, and scatterer density, so depending on the relative domination of these contents, c_1 will be determined.

The benefits of the proposed model was described as weighting by alpha increases the anisotropy of the diffusion process while improving edge preservation and speckle reduction [27]. Homogeneous regions will reduce the diffusion process to the case of Gaussian diffusion because these regions will result in a small value for the gradient and have few scatterers per resolution cell. Alternately, in the case of regions of high information contained in the gradient and scatterer density with different weights, especially at edges, interfaces, vessels, speckled and textured regions, the diffusion process is anisotropic as a function of these parameters, thus operating adaptively depending on the relative contents of these parameters in the locally analyzed regions.

B. Image quality measures

Image quality measures how far a processed image is from an original one (noisy or reference). The RMSE, SNR, and PSNR are image quality measures and are given as:

$$RMSE = \left(\frac{1}{NM}\sum_{i=1}^{N}\sum_{j=1}^{M}(u_{original}(i,j) - u_{denoised}(i,j))^2\right)^{1/2} \tag{35}$$

$$PSNR(dB) = 20\log_{10}(1/RMSE) \tag{36}$$

$$SNR(dB) = 10\log_{10}(\sigma_u^2/\sigma_e^2) \tag{37}$$

$$\sigma_e^2 = \left(\frac{1}{NM}\sum_{i=1}^{N}\sum_{j=1}^{M}|u_{original}(i,j) - u_{denoised}(i,j)|^2\right) \tag{38}$$

where σ_u^2 is the variance of the denoised image. When it comes to edginess, a quantitative value is required to measure how far the processed edges are from the reference one. FOM is a quantitative measure of edge preservation and enhancement [34], and is calculated from the Canny edge map:

$$FOM = \frac{1}{\max\{\hat{N}, N_{ideal}\}}\sum_{i=1}^{\hat{N}}\frac{1}{1 + d_i^2\lambda} \tag{39}$$

$\hat{N}$ is the number of edge pixels in the image and N_{ideal} is the number of edge pixels in the reference image. The term d_i represents the distance between the detected edge pixel, i, and the nearest reference edge pixel. In our calculation of the FOM we set the parameter λ to be 1/9 as in [17]. The FOM has a dynamic range of [0,1], with higher values indicating better edge matching between the processed and ideal images. In addition to these image quality measures, we calculated an image quality index (γ) [27], which measures the overall image and segmentation quality between two images. In our analysis, we computed γ as the product of the PSNR (with respect to the reference image) and the Pratt's figure of merit (FOM). Now we have quantitative measures of the image quality (PSNR, SNR, and RMSE), quality of edge preservation (FOM) and an overall index of image and segmentation quality (γ).

C. Diffusion Parameters

The value of τ in (32) is kept small to guarantee the solution to the diffusion equation be stable [37]. This is due to limitations in the non-ideal 3x3 stencil, A. The conductance parameter, K, is used to balance the amount of forward diffusion (smoothing the entire image) with backward diffusion (contrast enhancement over the entire image). We have tested the algorithm for different values of $\tau \leq 0.2$. We measured the quality of diffusion in SNR, PSNR, FOM, γ, α, the detected Canny edge map, the visual inspection of the diffused image, the 2D maps for α and gradient, and the

World Academy of Science, Engineering and Technology
International Journal of Medical and Health Sciences
Vol:1, No:5, 2007

evolution of the overall image average scatterer density (α_{avg}). For the case of coherence enhancing diffusion, we set the value of the constant, k to be 0.0001.

D. Proposed Stopping Functions

The actual value of the quality measures is not physically meaningful, but the comparison between two values for different diffused or reconstructed images gives one measure of reconstructed or processed quality [19]. Using PSNR measure for example in image reconstruction, the MPEG committee used an informal threshold of 0.5 dB PSNR to decide whether to incorporate a coding optimization since they believed that any improvement of that magnitude would be visible [19].

We propose using a difference of PSNR values at successive iterations to determine when to stop the filtering process. The value, δ, in dB, is calculated as:

$$\delta = PSNR^k - PSNR^{k-1} \qquad (40)$$

$PSNR^k$ represents PSNR between the processed image at iteration k and the original image (at $k = 0$). From experiment, we determined that a value of $\delta < 0.02$ dB corresponded to a processed image of sufficient visual quality.

In certain cases, a noise free image is available for quality measurements. In these special cases, the quality measures should be made between the ideal (noise free or reference) image and the processed image. It is in these cases that the value for γ is useful. The stopping function is proposed as [27]:

$$\delta_{ref}(\%) = \frac{\alpha_{avg}^k \gamma^k - \alpha_{avg}^{k-1} \gamma^{k-1}}{\alpha_{avg}^0 \gamma^0} * 100 \qquad (41)$$

α_{avg}^k is the average scatterer density at iteration k and γ^k is the overall quality index. The δ_{ref} value is given as a %.

E. Proposed Algorithm

An iteration k, of the proposed algorithm consists of the following steps:

Step 1) Convolve the image with G_σ of one standard deviation as in (18), $\tau = 0.2$.

Step 2) For each point (x,y) that belongs in the image, calculate the magnitude of the gradient, as in (5).

Step 3) Calculate the diffusivity function, $C(x,y,t)$ at iteration k, as in (34) for the whole image.

Step 4) Construct the matrices for the eigenvectors and eigenvalues, which depend on the method being implemented.

Step 5) Calculate the elements of the diffusion tensor matrix (a, b, and c).

Step 6) Calculate the elements for the 3 x 3 stencil $A_{i,j}^k$ (Fig. 1) and 'convolve' with the image at iteration k and multiply resultant matrix by τ.

Step 7) Solve for $u_{i,j}^{k+1}$ using:

$$u_{i,j}^{k+1} = u_{i,j}^k + \tau(A_{i,j}^k * u_{i,j}^k) \qquad (42)$$

Step 8) Loop until desired image quality is obtained (δ) or until maximum discrete time steps, T_{max}, is reached.

VII. EXPERIMENTAL RESULTS AND EVALUATION

We investigated and tested the performance of the proposed SWDNLD for the tensor based cases of EED and CED in reducing the speckle noise for test phantom and clinical ultrasound images using two weighting parameters: the image gradient and the scatterer density, α. We tested the performance using two methods. First, we used only the traditional case, in which the diffusivity function includes only the gradient. Second, we altered the diffusivity function as suggested in Eq. (33) by weighting the gradient with the scatterer density. In each case and for each iteration, the SNR, PSNR, FOM and γ were calculated for the processed image. Also, Canny edge maps, gradient maps, and scatterer density maps were generated, and the average scatterer density, α_{avg} was calculated. The default diffusion parameters were set to $\sigma = 1$, $K = 0.01$, $\tau = 0.2$, $T = 9$, and the number of iterations was set to 45 for comparisons, using the Perona Malek 1 diffusivity function, and a 3x3 window. In the coherence enhancing case, $k = 0.0001$.

A. Images used for testing and evaluation

In our experiments, we used a contrast detail phantom image (ATS laboratories, Bridgeport, CT). The contrast detail phantom was made to produce standard contrast levels from −15 dB to +12 dB. The phantom image has a resolution of 256x128 and consists of eight different contrast regions (four positive contrast regions and four negative contrast regions). Regions are ordered in two rows. The upper row contains negative contrast regions while the lower one contains positive contrast regions as shown in Fig. 2. A reference image was constructed manually from the speckled image by evaluating the mean value in each region. All phantom and clinical images were acquired at frequency of 3.5 Mhz. Fig. 2 shows an original contrast detail phantom (a), its Canny edge map (b), its scatterer density map (c), Reference contrast detail phantom (d), its Canny edge map (e), and its scatterer density map (f). Images in Figs. 2.b and 2.c show how these gradient and scatterer density feature maps are vague and do not correspond to the underlying structures. Figs. 2.e and 2.f show how these image feature maps are clear and correspond to the underlying structure. That is the role of this novel proposed work to make the resulted speckle reduced images preserve the underlying structures.

B. Scatterer density weighted nonlinear edge enhancing diffusion (SDWNEED)

In this model of EED, we used the tensor based formulation described in Eqs. (19)-(21), to test and evaluate the enhancements increased by incorporating scatterer density into diffusivity function. In this case, $\lambda_2 = 1$ and $\lambda_1 = C(x,y,t)$.

B.1 Results of SDWNEED for contrast detail image

Fig. 3 shows the progressions of the diffused images and their Canny edge maps for 45 iterations of $\tau = 0.2$ at intervals corresponding to T = 1, 3, 6 and 9 (5, 15, 30 and 45 iterations). Fig. 4 shows the corresponding Canny edge maps. From the figures we see that, visually, the images become clearer in the region around T = 6 – 9. Also, the Canny edge maps, which begin as vague and meaningless in the first iteration, start to show meaningful edge features as the

World Academy of Science, Engineering and Technology
International Journal of Medical and Health Sciences
Vol:1, No:5, 2007

diffusion process progresses. The circular patterns of the phantom images begin to appear clearly around T = 6. Notice that by visual inspection alone, the Canny edge maps at T = 6 and 9 in Fig. 4 are much closer to the Canny edge map for the reference image than the map in Fig. 2b. Quantitatively speaking, the FOM progresses from 0.181 at T = 1, to 0.2124, 0.2604, and finally to 0.3242, indicating the overall increase in segmentation quality with the progression of the filtering process. Fig. 5 shows the gradient and scatterer density maps at T = 1 and T = 9. With the evolution of the process in time, we see the gradient and scatterer density maps progress from vague to clearly showing image features that correspond to the anatomical underlying structures in the image. The overall scatter density (α_{avg}) progressively decreases from 0.3231 (T = 0), 0.2537, 0.1907, 0.1515, 0.1329 (T = 1, 3, and 9). The values of γ were 4.367, 4.566, 5.646, 7.15, 9.028 (T = 0,1,3,6 and 9). These values illustrate the increase in overall image and segmentation quality with time.

B.2 Choice of Conductance Parameter, K, on SDWNEED

For large values of K ($K \geq (\alpha|\nabla u|)$), the diffusivity function reduces to linear diffusion, where the entire image is smoothed at the cost of edge preservation. For small values ($K \leq (\alpha|\nabla u|)$), the diffusion process exhibits edge preservation at the cost of speckle noise reduction. The conductance parameter, K, can be used as a time varying function as in [20] in order to cool down the system. The value of K is used to balance the amount of forward diffusion (where everything is smoothed) and backward diffusion (where contrast enhancement is happened). Ideally, K will be chosen to balance these two properties to reduce speckle noise and preserve edges. Choosing K was done by applying edge enhancing diffusion for 25 iterations (T = 5). Fig. 8 shows the graphs of the image and segmentation quality measurements for various values of the conductance parameter. From Fig. 8 we see that, for very small K (< 0.05), the values for PSNR, FOM, α_{avg}, and γ change rapidly with K, indicating values of K corresponding to high contrast enhancement. For larger values of K (≥ 0.05), there is little change in the values of the image and segmentation quality measurements, indicating approximately linear image smoothing for these values of K.

TABLE I
COMPARING FOM, α_{avg}, PSNR, AND γ FOR DIFFERENT CHOICES OF CONDUCTANCE PARAMETER, K FOR SDWNEED ($\lambda_2 = 1$).

K	FOM	α_{avg}	PSNR$_{ref}$	γ
0.001	0.1861	0.2094	25.17	4.684
0.005	0.217	0.169	26.63	5.781
0.01	0.2254	0.1609	27.25	6.142
0.05	0.2648	0.1609	27.63	7.316
0.1	0.2503	0.1619	27.63	6.916
0.2	0.2442	0.1618	27.62	6.746
0.3	0.2677	0.1617	27.62	7.395
0.4	0.2663	0.1616	27.62	7.355
0.5	0.2666	0.1617	27.62	7.363
1	0.2643	0.1616	27.62	7.300

Figs. 6-7 show the diffused images and its associated Canny maps after 25 iterations for various values of K. Values of $K \geq$ 0.05 display much smoothing across edges – an undesirable quality. The image corresponding to $K = 0.001$ has too little noise reduction, also undesirable. After 25 iterations, the image corresponding to $K = 0.01$ displays the ideal combination of noise reduction and edge preservation. The values for the FOM, α_{avg}, PSNR, and γ, is shown in Table I.

B.3 SDWNEED in removing noise and preserving edges

The noise removal and edge preservation performance of SDWNEED was measured by adding Gaussian noise ($\sigma = 20$) to three ultrasound test images – a fetal face test image (Fig. 9 of 433 x 580 pixels), a heart image (Fig. 10 of 256 x 256 pixels), and a phantom reference image (Fig. 11 of 256 x 128 pixels). The diffusion parameters used to test the effectiveness of our method were, $\sigma = 1$, $\tau = 0.2$, $K = 0.01$, T = 3, using the Perona-Malek 1 equation and was solved using the explicit method described previously with a 3 x 3 window.

The effectiveness of noise removal on image quality was measured quantitatively using different quality measures and was measured qualitatively using visual judgments of the 2D maps for Canny edge detection, the gradient, the scatterer density and using the diffused images. Tables II and Figs. 12-14 clearly illustrate the ability of the SDWNEED diffusion filter to reduce noise while preserving image features. The values in Tables II show that the filter improved image quality and increased edge segmentation in every case, most notably in the case of the phantom image. Clearly, segmenting the noisy images in Figs. 9(b), 10(b), and 11(b) would be no easy task. However, after applying the proposed method, image features become visible in the 2D Canny edge maps, allowing more accurate segmentation.

TABLE II
EFFECT OF SDWNLD ON SNR AND PSNR FOR SDWNEED ($\lambda_2 = 1$).

Image	SNR	PSNR
Face before denoising	2.784	19.406
Face after denoising	7.062	24.180
Heart before denoising	4.926	18.726
Heart after denoising	8.611	22.410
Phantom before denoising	-2.818	20.635
Phantom after denoising	12.75	36.290

B.4 Effect of scatterer density in weighting SDWNEED

We compare the effectiveness of the proposed SDWNEED with traditional EED. With scatterer density weighting, we modify λ_1 by:

$$\lambda_1 = C(x, y, t) = 1/(1 + \frac{(\alpha|\nabla U_\sigma|)^2}{K^2}) \qquad (43)$$

The parameters for the diffusion were chosen as $\sigma = 1$, $\tau = 0.2$, $K = 0.01$, T = 9, using the Perona-Malek 1 equation and was solved using the explicit method described previously with a 3 x 3 window. Table III and Figs. 27-28 show the improvement in image and segmentation quality obtained both quantitatively and visually with scatterer density weighting. From this we can conclude that weighting with the scatterer density is preferable to using the gradient only. It should be noted that the better quantitative performance after inclusion of the scatterer density in the diffusivity equation is expected.

World Academy of Science, Engineering and Technology
International Journal of Medical and Health Sciences
Vol:1, No:5, 2007

Using only one measure of the image features, the gradient in this case, is unwise because the gradient will contain noisy information, causing inaccurate edge preservation and geometric distortion. By including physical image characteristics, such as scatterer density, the process becomes more robust and results in better feature enhancement.

TABLE III
SNR, PSNR, FOM, γ, AND α_{avg} FOR TWO CHOICES OF DIFFUSIVITY
PARAMETERS FOR PHANTOM CONTRAST IMAGE FOR SDWNEED ($\lambda_2 = 1$).

Weighting	SNR_{ref}	$PSNR_{ref}$	FOM	γ	α_{ov}
$\lvert \nabla U_\sigma \rvert$	2.959	26.53	0.2092	5.544	0.1532
$\lvert \nabla U_\sigma \rvert.\alpha$	4.307	27.85	0.3242	9.028	0.1329

B.5 Evolution of SDWNEED for large number of iterations

We compare the performance of traditional edge enhancing diffusion to SDWNEED for a large number of iterations (150). Fig. 15 shows that SDWNEED performs the equivalent operation as traditional anisotropic diffusion in fewer iterations. From visual inspection it is apparent that with SDW diffusion, the ideal stopping point is T=9 (45 iterations). Here we reach an image displaying excellent speckle reduction without too much diffusion along the edges (PSNR = 27.85 dB, FOM = 0.3242). Examining the graphs of PSNR and FOM in Fig. 15 we see that it takes 116 iterations without SDW to reach the equivalent image quality and 114 iterations to reach approximately identical edge segmentation quality.

B.6 SDWNEED automatic stopping criteria evaluation

Fig. 16 shows the value of δ for several iterations of SDWNEED. The stopping criteria, δ < 0.02 is reached at iteration 46, which can be seen in Fig. 16. The image quality indicates much speckle reduction, as well as better edge preservations, with $PSNR_{ref}$ = 27.86 and FOM = 0.3318. Also, from the graph we see that the stopping criteria is reached with fewer iterations with SDW (46 iterations with SDW compared to 74 without SDW) which indicates that SDWNEED is able to perform much faster than traditional EED.

C. Scatterer density weighted nonlinear coherence enhancing diffusion (SDWNCED)

In this model of SDWNCED, we used the tensor based formulation described in Eqs. (23)-(34), to test and evaluate the SDWNCED performance compared to the traditional CED when incorporating scatterer density into the diffusivity function.

C.1 Results of SDWNCED for contrast detail image

Figs. 17-18 shows the progressions of the diffused images and their Canny edge maps for 45 iterations of τ = 0.2 at intervals corresponding to T = 1, 3, 6 and 9 (5, 15, 30 and 45 iterations). Fig. 18 shows the corresponding Canny edge maps. From the figures we see that, visually, the images become clearer in the region around T = 6 − 9. Also, the Canny edge maps, which begin as vague and meaningless in the first iteration, start to show meaningful edge features as the diffusion process progresses. The circular patterns of the phantom images begin to appear clearly around T = 6. Notice

that by visual inspection alone, the Canny edge maps at T = 6 and 9 in Fig. 18 is much closer to the Canny edge map for the reference image than the beginning map. Quantitatively speaking, the FOM progresses from 0.1769 at T = 1, to 0.2087, 0.2475, and finally to 0.3177, indicating the overall increase in segmentation quality with the evolution of the filtering process. Fig. 19 shows the gradient and scatterer density maps at T = 1 and T = 9. With the evolution of the process in time, we see the gradient and scatterer density maps progress from vague to clearly showing image features. The overall scatter density (α_{avg}) progressively decreases from 0.3231 (T = 0), 0.2541, 0.1861, 0.1489, 0.1317 (T = 1, 3, 6, and 9). The values of γ were 4.336, 4.495, 5.579, 6.812, 8.851 (T = 0,1,3,6 and 9). These values illustrate the increase in overall image and segmentation quality with time.

C.2 Choice of conductance parameter, K, on SDWNEED

To determine the ideal value for the conductance parameter, K, experiment in section B.2 was repeated and it was found that K = 0.01 also display the ideal combination of noise reduction and feature preservation. Figs. 23-24 show the resulted images.

C.3 SDWNCED in removing noise and enhancing coherency

The noise removal and edge preservation performance of SDWNCED was measured by using the same test images as used in the edge enhancing case. The diffusion parameters used to test the effectiveness of our method were, σ = 1, τ = 0.2, K = 0.01, T = 3, k = 0.0001 using the Perona-Malek 1 equation and was solved using the explicit method described previously with a 3 x 3 window. Table IV and Figs. 20-22 clearly illustrate the ability of the SDWNCED filter to reduce noise while preserving image features.

TABLE IV
EFFECT OF SDWNLD ON SNR AND PSNR FOR THE SDWNCED.

Image	SNR_{ref}	$PSNR_{ref}$
Face before denoising	2.784	19.406
Face after denoising	6.641	23.758
Heart before denoising	4.926	18.726
Heart after denoising	8.209	22.008
Phantom before denoising	-2.818	20.635
Phantom after denoising	11.970	35.423

The values in Table IV show that the filter improved image quality and increased edge segmentation in every case, most notably in the case of the phantom image. Again, accurately segmenting the noisy images in Figs. 9(b), 10(b), and 11(b) would be no easy task. After applying the proposed method, image features become visible in the 2D Canny edge maps, allowing more accurate segmentation.

C.4 Effect of scatterer density in weighting SDWNCED

We compare the effectiveness of the proposed SDWNCED with traditional CED. For this case, c_2 is modified to include the scatterer density:

$$c_2 = C(x, y, t) = C(\alpha \lvert \nabla u \rvert) \qquad (44)$$

Also, c_1 remains as described by Eq. (26). The parameters for the diffusion were chosen as σ = 1, τ = 0.2, K = 0.01, T = 9, k

World Academy of Science, Engineering and Technology
International Journal of Medical and Health Sciences
Vol:1, No:5, 2007

= 0.0001 using the Perona-Malek 1 equation and was solved using the explicit method described previously with a 3 x 3 window. Table V and Figs. 27-28 show the improvement in image and segmentation quality obtained both quantitatively and visually with scatterer density weighting. From this we can conclude that weighting with the scatterer density is preferable to using the gradient only in the formulation of c_2. Also we see from Figs. 27-28 that both the gradient only and SDW method are preferable to using $c_2 = 0.01$.

TABLE V
SNR, PSNR, FOM, γ, AND $α_{avg}$ OF THE DIFFUSED IMAGES FOR THREE CHOICES OF DIFFUSIVITY PARAMETERS WEIGHTING IN SDWNCED.

Weighting	SNR_{ref}	$PSNR_{ref}$	FOM	γ	$α_{ov}$
$\|\nabla U_\sigma\|$	3.52	27.06	0.2037	5.512	0.1482
$\|\nabla U_\sigma\|.\alpha$	4.316	27.86	0.3177	8.851	0.1317
$c_2 = 0.01$	2.611	26.15	0.1646	4.304	0.2062

C.5 Evolution of SDWNCED for large number of iterations

We compare the performance of traditional coherence enhancing diffusion to this case of SDWNCED for a large number of iterations (150). Fig. 25 shows that SDW diffusion performs the equivalent operation as traditional anisotropic diffusion in fewer iterations. From visual inspection it is apparent that with SDW diffusion, the ideal stopping point is T=9 (or after 45 iterations). Here we reach the best image quality, displaying much speckle reduction without too much diffusion along the edges (PSNR = 27.86 dB, FOM = 0.3177). Examining the graphs of PSNR and FOM in Fig. 25 we see that it takes over 150 iterations using the traditional filtering method to reach the equivalent image quality and 147 iterations to reach approximately identical edge segmentation quality.

C.6 SDWNCED Automatic stopping criteria evaluation

Fig. 26 shows the value of δ for 150 iterations of SDWNCED. The stopping criteria, δ < 0.02 is reached at iteration 46, which can be seen in Fig. 26. The image quality displays an excellent balance of speckle reduction and feature preservation with $PSNR_{ref}$ = 27.87 and FOM = 0.3251. Also, from the graph we see that the stopping criteria is reached with fewer iterations with SDW (46 iterations w/ SDW compared to 64) which indicates that SDWNCED is able to perform much faster that traditional CED.

D. Comparison between SDWNEED, SDWNCED, and some other speckle reduction methods

The performance of the two methods proposed in this section was compared to the performance of some other diffusion methods such as NCD, SRAD (at time step τ=0.2 and for 45, 100, and 150 iterations), AWMF, WS, WSCE, and SDWND. Both SDWNEED (using λ2 = 1 and λ2 = C(x,y,t)/5 cases) and SDWNCED were performed using K = 0.01 and stopped using the stopping criteria mentioned earlier. The value for γ obtained using these new methods was also much higher, indicating the better overall image and segmentation quality obtained using SDWNEED and SDWNCED. Table VI

shows the values for the SNR, PSNR, FOM and γ obtained using the various methods (using PSNR with respect to original image at T = 0 and FOM with respect to Canny reference image).

Qualitatively, the resulting images, their Canny edge maps, and scatterer density maps are compared in Figs. 29-31. From Fig. 29, it can be seen that the SDWNEED and SDWNCED methods achieved excellent speckle reduction while preserving image features. This result is reinforced in Fig. 30, where it can be seen from the Canny edge maps that the methods presented achieved preservation of image features observed in having the best circular edge structures of the phantom image compared to other methods thus better preserving the underlying anatomical structures.

TABLE VI
COMPARISON OF SNR, PSNR, FOM AND γ FOR DIFFUSED IMAGES WITH SDWNEED, SDWNCED, SDWND, NCD, SRAD, AWMF, WS, AND WSCE METHODS.

Method	SNR	PSNR	FOM	γ
SDWNEED (λ2 = C(x,y,t)/5)	3.587	23.85	0.311	7.417
SDWNEED (λ2 = 1)	3.567	23.831	0.332	7.911
SDWNCED	3.517	23.781	0.325	7.728
SDWND	4.379	24.646	0.216	5.323
NCD	3.618	23.885	0.200	4.777
SRAD-45	2.790	23.057	0.199	4.588
SRAD-100	2.031	22.298	0.252	5.619
SRAD-150	1.800	22.067	0.294	6.487
AWMF	3.712	23.979	0.184	4.412
WS	4.127	24.393	0.171	4.171
WSCE	3.150	23.468	0.177	4.153

TABLE VII
COMPARISON OF SNR_{aref} AND $PSNR_{aref}$ FOR SCATTERER DENSITY IMAGES IN FIG. 31 WITH SDWNEED, SDWNCED, SDWND, NCD, AWMF, WS, AND WSCE METHODS.

Method	SNR_{aref}	$PSNR_{aref}$
Before denoising	-17.497	9.222
SDWNEED (λ2 = C(x,y,t)/5)	-10.760	15.959
SDWNEED(λ2 = 1)	-10.890	15.824
SDWNCED	-10.825	15.890
SDWND	-11.800	14.973
NCD	-11.820	14.899
SRAD-45	-13.749	11.801
SRAD-100	-12.242	13.309
SRAD-150	-11.474	14.077
AWMF	-13.578	13.141
WS	-14.321	12.399
WSCE	-16.495	10.224

Table VII show the SNR and PSNR calculated with the reference scatterer density map of Fig. 2.e. Fig. 31 show the scatterer density map with different compared method. Fig. 31 and Table VII show quantitatively how the scatterer density as a physical parameter is much preserved when we weight the anisotropic diffusion with the scatterer density in terms of *SNR* and *PSNR*. As shown in Table VII, the highest four values for the scatterer density PSNR are for the three anisotropic methods discussed and shown in the last row of Fig. 29, and the isotropic method discussed in [27] which used the scatterer density weighting method in isotropic diffusion.

In summary, both SDWNEED and SDWNCED methods perform better over the NCD, SRAD, AWMF, WS, WSCE,

and SDWND methods in reducing speckle and preserving image features such as edges of the geometrical circular structures and scatterer density distribution over the whole image. The improvements can be seen both quantitatively (Tables VI-VII) and qualitatively (Figs. 29-31). When compared with each other, SDWNCED and SDWNEED for corresponding SNR, PSNR, FOM and γ values, there was little discernible difference between these measures and the resultant images. Figs. 29-30 show that SDWNCED perform slightly better than SDWNEED in terms of the circularity of the diffused circle. This slight advantage of SDWNCED over SDWNEED is because SDWNCED combines speckle reduction, edge preservation, scatterer density preservation in addition to coherence enhancement of geometrical structures as in the case of the phantom circles.

VIII. DISCUSSION AND CONCLUSIONS

This work proposes new enhancement methods to the traditional tensor based formulations of EED and CED which effectively reduce speckle while preserving important image features as the edges, coherent structures, and scatterers density distribution that correspond to the underlying anatomical structure. Also suggested is a new index for establishing the overall image and segmentation quality (γ), which is the product of the FOM and the PSNR. For each method, the extent to which the method reduced speckle noise was examined using an ultrasound phantom image. SDWNEED and SDWNCED cases performed well, showing improvements in image and segmentation quality. Second, an optimal choice for the conductance parameter, K, was tuned to balance noise reduction with feature preservation. To test speckle reduction and features preservation, each filtering method was then used to process various ultrasound images with added Gaussian noise. Both filters showed improvements in image quality in all cases. Third, the effect of scatterer density weighting was compared with the conventional case for each filter. SDW showed improvements in image and segmentation quality over the traditional method that uses only gradient information. Fourth, the effect of SDW was examined for a large number of iterations, in this case 150. Both SDWNEED and SDWNCED methods showed an improvement over traditional methods in speed, requiring less iteration to obtain images of similar quality.

These experiments confirm that the introduction of scatterer density into the cases of EED and CED increase the performance of these filters in both noise reduction and feature preservation. The proposed methods could succeed to balance between speckle suppression and features preservation (edges, coherence, and scatterer density distribution) as it is clear that the resulted diffused images are preserving the underlying structures in terms of edges, coherence, and scatterer density distribution. To summarize, the proposed filters are speckle reducing, scatterer density weighted edge and coherence enhancing filters. These methods are ideal for preprocessing of ultrasound images for automatic segmentation, as in the accurate preservation of image features which anatomically correspond to the underlying structures and thus allow for more accurate segmentation. The NCD and SRAD limitation

or none being able to retain subtle features due to regarding the size of speckle that may occupy more than the size of a pixel was overcame in our formulation by taking HxW window to calculate scattered density along local larger windows in the image.

In summary, the proposed SDWNEED and SDWNCED methods performed better over the NCD, SRAD, AWMF, WS, WSCE, and SDWND methods in reducing speckle and preserving overall image features such as edges of the geometrical circular structures and scatterer density distribution over the whole image.

REFERENCES

[1] M. E. Anderson, and G. E. Trahey, "A seminar on k-space applied to medical ultrasound," *http://dukemil.egr.duke.edu/Ultrasound/k-space/* (Accessed July 1, 2006).
[2] J. C. Bamber and C. Daft, "Adaptive filtering for reduction of speckle in ultrasound pulse-echo images," Ultrasonics, pp. 41–44, Jan. 1986.
[3] T. Iwai, T. Asakura, "Speckle reduction in coherent information processing," Proceedings of the IEEE, vol. 84, no. 5, 1996.
[4] V. Dutt, "Statistical analysis of ultrasound echo envelope," Ph.D. dissertation, Mayo Graduate School, Rochester, MN, 1995.
[5] D. Blacknell, "Comparison of parameter estimators for K-distribution," IEE Proceedings – Radar, Sonar Navigation, vol. 141, pp. 45–52, Feb. 1994.
[6] J. C. Bamber and G. Cook-Martin, "Texture analysis and speckle reduction in medical echography," SPIE, pp. 120-127, 1987.
[7] Perona, P. and J. Malik, "Scale-space and edge detection using anisotropic diffusion," Proceedings, IEEE Computer Society workshop on Computer Vision, 1987, pp. 16-27.
[8] P. Perona and J. Malik, "Scale space and edge detection using anisotropic diffusion," IEEE Trans. Pattern Anal. Machine Intell., vol. 12, pp. 629–639, July 1990.
[9] M. J. Black, G. Sapiro, D. H. Marimont, and D. Heeger, "Robust anisotropic diffusion," IEEE Trans. Imag. Processing, vol. 7, pp. 412–432, Mar. 1998.
[10] J.Weickert, "Mutiscale texture enhancement," in Lecture Notes in. Computer Science, ser. Berlin, vol. 970, Computer Analysis of Images and Patterns, pp. 230–237, 1995.
[11] J. Weickert et al., "Efficient and reliable schemes for nonlinear diffusion filtering," IEEE Trans. Imag. Processing, vol. 7, pp. 398–410, Mar. 1998.
[12] K. Z. Abd-Elmoniem, Y. M. Kadah, and A. M. Youssef, "Real time adaptive ultrasound speckle reduction and coherence enhancement," presented at the Int. Conf. Imag. Processing (ICIP' 2000), Vancouver, Canada, 2000.
[13] K.Z. Abd-Elmoniem, A. M. Youssef, and Y. M. Kadah, "Real-time speckle reduction and coherence enhancement in ultrasound imaging via nonlinear anisotropic diffusion," IEEE Transaction on Biomedical Engineering, vol. 49, no. 9, pp. 997-1014, 2002.
[14] A. Achim, A. Bezerianos, and P. Tsakalides, "Novel Baysian multiscale method for speckle removal in medical ultrasound images," IEEE Trans. Medical Imaging, vol. 20, pp. 772–783, Aug. 2001.
[15] R. A. Carmona and S. Zhong, "Adaptive smoothing respecting feature directions," IEEE Trans. Image Processing, vol. 7, pp. 353–8, Mar. 1998.
[16] Weeratunga S.K. and C. Kamath, "PDE-based non-linear diffusion techniques for denoising scientific/industrial images: An empirical

World Academy of Science, Engineering and Technology
International Journal of Medical and Health Sciences
Vol:1, No:5, 2007

study," Proceedings, Image Processing: Algorithms and Systems, SPIE Electronic Imaging, pp. 279-290, San Jose, January 2002.

[17] Weeratunga S.K., and C. Kamath, "A comparison of PDE-based non-linear anisotropic diffusion techniques for image denoising," Proceedings, Image Processing: Algorithms and Systems II, SPIE Electronic Imaging, San Jose, January 2003.

[18] P. M. Shankar, "A general statistical model for ultrasonic backscattering from tissues," IEEE Trans. Ultrason. Ferroelect. Freq. Contr., vol. 47, pp. 727–736, Mar. 2000.

[19] A.N. Netravali and B.G. Haskell, Digital pictures: representation, compression, and standards (2nd Ed), Plenum Press, New York, NY (1995).

[20] G. Gilboa, Y.Y. Zeevi, N. Sochen," Image enhancement segmentation and denoising by time dependent nonlinear diffusion processes," Proceedings. 2001 International Conference on Image Processing, vol. 3, pp. 134 – 137, Oct. 2001.

[21] R. Touzi, "A review of speckle filtering in the context of estimation theory," IEEE Trans. Geosci. Remote Sens., vol. 40, no. 11, pp. 2392–2404, Nov. 2002.

[22] J. Lee, "Digital image enhancement and noise filtering using local statistics," IEEE Trans. Pattern Anal. Mach. Intell., vol. PAMI-2, no. 2, pp. 165–168, Mar. 1980.

[23] V. Frost, J. Stiles, K. Shanmugan, and J. Holzman, "A model for radar images and its application to adaptive digital filtering of multiplicative noise," IEEE Trans. Pattern Anal. Mach. Intell., vol. PAMI-4, no. 2, pp. 157–166, Mar. 1982.

[24] D. T. Kuan, A. A. Sawchuk, T. C. Strand, and P. Chavel, "Adaptive noise smoothing filter for images with signal-dependent noise," IEEE Trans. Pattern Anal. Mach. Intell., vol. PAMI-7, no. 2, pp. 165–177, Mar. 1985.

[25] D. T. Kuan, A. A. Sawchuk, T. C. Strand, and P. Chavel, "Adaptive restoration of images with speckle," IEEE Trans. Acoust., Speech, Signal Process., vol. ASSP-35, no. 3, pp. 373–383, Mar. 1987.

[26] Y. Yu and T. Acton, "Speckle reducing anisotropic diffusion," IEEE Trans. On Image Processing, vol. 11, No. 11, pp. 1260-1270, November 2002.

[27] A. Badawi, "Scatterer density in nonlinear diffusion for speckle reduction in ultrasound imaging: the isotropic case," International Journal of Biomedical Sciences, vol. 2, No. 3, 2007.

[28] X. Hao, C. Bruce, C. Pislaru, and J. Greenleaf, "Identification of reperfused infracted myocardium from high frequency intracardiac ultrasound images using homodyned K distribution," IEEE Ultrasonics Symposium, pp. 1189-1192, 2001.

[29] X. Hao, C. Bruce, C. Pislaru, and J. Greenleaf, "Characterization of reperfused infracted myocardium from high-frequency intracardiac ultrasound images using homodyned K distribution," IEEE Transaction on Ultrasonics, Ferroelectric, and Frequency Control, vol. 49, no. 11, pp. 1530-1542, November 2002.

[30] R. Smolikova, M. Wachowiak, G. Tourassi, and J. Zurada "Neural estimation of scatterer density in ultrasound," Proceedings of the 2002 International Joint Conference on Neural Networks, vol. 2, pp. 1696 – 1701, 12-17 May 2002.

[31] M. Rabbani and P.W. Jones, Digital image compression techniques, vol. TT7, SPIE Optical Engineering Press, Bellvue, Washington (1991).

[32] Z. Yang and M. Fox, "Speckle reduction and structure enhancement by multichannel median boosted anisotropic diffusion," EUROASIP Journal on Applied Signal Processing, vol. 16, pp. 2492-2502, 2004.

[33] R. V. D. Boomgaard, Algorithms for non-linear diffusion Matlab in a literate programming style, Intelligent Sensory Information Systems, University of Amsterdam, The Netherlands http://carol.wins.uva.nl/~rein/nldiffusionweb/material.html (Accessed Feb. 2007).

[34] W. K. Pratt, Digital Image Processing, Wiley, New York, NY, USA, 1978.

[35] J. Weickert, "Anisotropic Diffusion in Image Processing," PhD dissertation, Kaiserslautern University, Germany, 1996.

[36] J. Weickert, "Coherence-Enhancing Diffusion Filtering," International Journal of Computer Vision, vol. 31(2/3), pp 111-127, 1999.

[37] J Weickert. "A Scheme for Coherence-Enhancing Diffusion Filtering with Optimized Rotation Invariance," Journal of Visual Communication and Image Representation, vol. 13, pp 103-118, 2002.

[38] T. Loupas, W. N. Mcdicken, and P. L. Allan, "An adaptive weighted median filter for speckle suppression in medical ultrasonic images," IEEE Trans. Circuits Syst., vol. 36, no. 1, pp. 129–135, Jan. 1989.

[39] Z. Yang and M. Fox, "Speckle reduction and structure enhancement by multichannel median boosted anisotropic diffusion", EUROASIP Journal on Applied Signal Processing, vol. 16, pp. 2492-2502, 2004.

Ahmed Badawi (M'05-SM'06) received his BSC, MSC, PhD in 1990, 1993, and 1996 respectively from Department of Systems & Biomedical Engineering, Cairo University. He was an assistant professor, associate professor, and full professor in 1996, 2001, and 2007 respectively at Systems & Biomedical Engineering Cairo University. He is a visiting professor at University of Tennessee, Biomedical Engineering Department since August 2005. He is a professor on leave at Systems & Biomedical Engineering, Cairo University.

His research interests are in Medical Imaging, 3D/4D Ultrasound Scanning, Reconstruction, Visualization, and Measurements, 4D Surgical Navigation, Image Processing, Computer Vision and Pattern Recognition in Medicine, Neural Networks, Fuzzy Systems, Medical Classification, Biometrics, Intelligent Medical Systems, Medical Software Workstations. He is a reviewer of several international journals, chairman of several international conferences sessions and track chairman.

Dr. Badawi is a senior member, IEEE, a member in IEEE Engineering in Medicine and Biology society. Dr. Badawi published over 75 papers in journals and peer reviewed conferences. He awarded several prestigious awards such as Egyptian National Academy for Scientific Research and Technology, Cairo University award for Engineering Research. Dr. Badawi was a director of Imaging Solutions Department at ibetech.com where he was the head of the team who developed the first 3D ultrasound system in Egypt. Dr. Badawi has over 17 years experience in Systems & Biomedical Engineering teaching and research. Dr. Badawi supervised over 20 MSC and PhD students.

J. Michael Johnson received his BSC in 2006 from the Whiting School of Engineering, Johns Hopkins University. His research interests include Medical imaging and enhancement, Computer vision, and Computer-aided diagnostics. Currently, he is a PhD candidate and Research Assistant under Dr. Mohamed Mahfouz in the Department of Mechanical, Aerospace, and Biomedical Engineering, University of Tennessee Knoxville.

Mohamed Mahfouz (M'02-SM'06) received his BSC, MSBME, in 1987, 1992, respectively from Department of Systems & Biomedical Engineering, Cairo University. He received his MSEE in 1997 from University of Denver, CO. He received his PhD in 2002 from Colorado School of Mines, CO. He is associate professor of Biomedical Engineering at University of Tennessee, Knoxville. His research interests are in Biomedical instrumentation, Medical imaging and enhancement, Surgical navigation, Advanced visualization, Orthopedic dynamic modeling, 3D bone and tissue reconstruction, Vascular computational fluid dynamics, Engineering analysis of surgical techniques and outcomes, and Anthropomorphic classification. He is a reviewer of several international journals and chairman of several international conference sessions.

Dr. Mahfouz is a senior member, IEEE, a member in IEEE Engineering in Medicine and Biology society, IEEE computer society, Orthopaedic Research Society (ORS), American Association for the Advancement of Science (AAAS), and International Society of Technology in Arthroplasty (ISTA). Dr. Mahfouz published over 100 papers in journals and peer reviewed conferences. Dr. Mahfouz worked in IBM as an I/T architect, Colorado, Denver, in Ratheon, Englewood, Colorado, as Engineering project manager, and is currently a co-director of CMR lab. Dr. Mahfouz supervised over 30 MSC and PhD students. Dr. Mahfouz has over 20 years experience in Systems & Biomedical Engineering.

World Academy of Science, Engineering and Technology
International Journal of Medical and Health Sciences
Vol:1, No:5, 2007

$\dfrac{b_{i-1,j} - b_{i,j+1}}{4}$	$\dfrac{c_{i,j+1} + c_{i,j}}{2}$	$\dfrac{b_{i+1,j} + b_{i,j+1}}{4}$
$\dfrac{a_{i-1,j} + a_{i,j}}{2}$	$-\dfrac{a_{i-1,j} + 2a_{i,j} + a_{i+1,j}}{2} - \dfrac{c_{i,j-1} + 2c_{i,j} + c_{i,j+1}}{2}$	$\dfrac{a_{i+1,j} + a_{i,j}}{2}$
$\dfrac{b_{i-1,j} + b_{i,j-1}}{4}$	$\dfrac{c_{i,j-1} + c_{i,j}}{2}$	$\dfrac{b_{i+1,j} - b_{i,j-1}}{4}$

Fig. 1 The standard discretization for the 3x3 stencil, A.
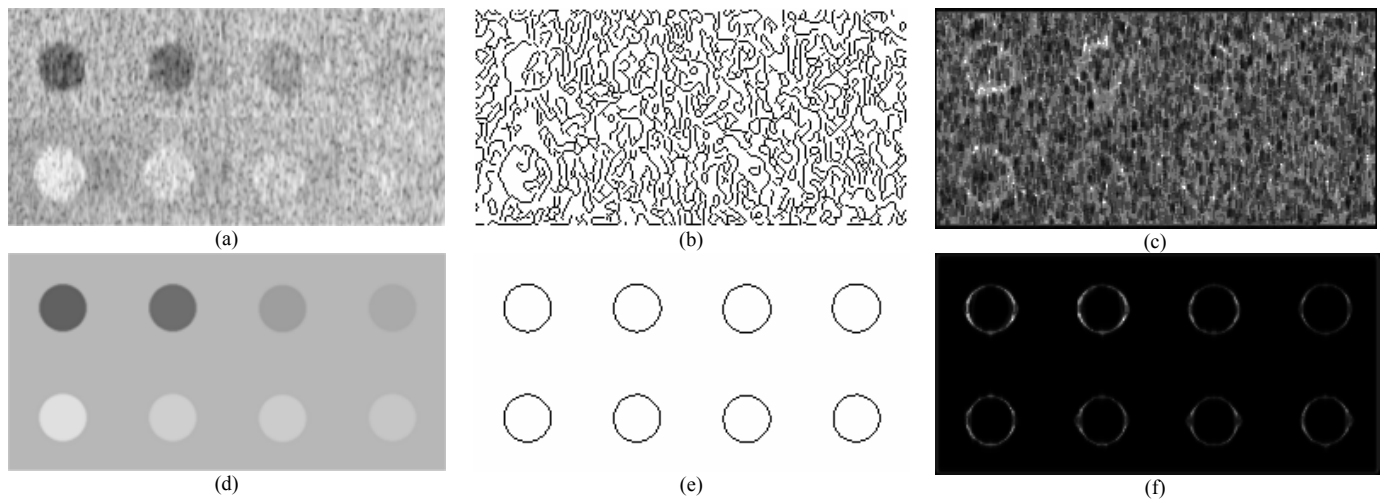
Fig. 2 Contrast detail phantom of resolution 256x128 (a), its Canny edge map (b), its scatterer density map (c), Reference contrast detail phantom (d), its Canny edge map (e), and its scatterer density map (f).
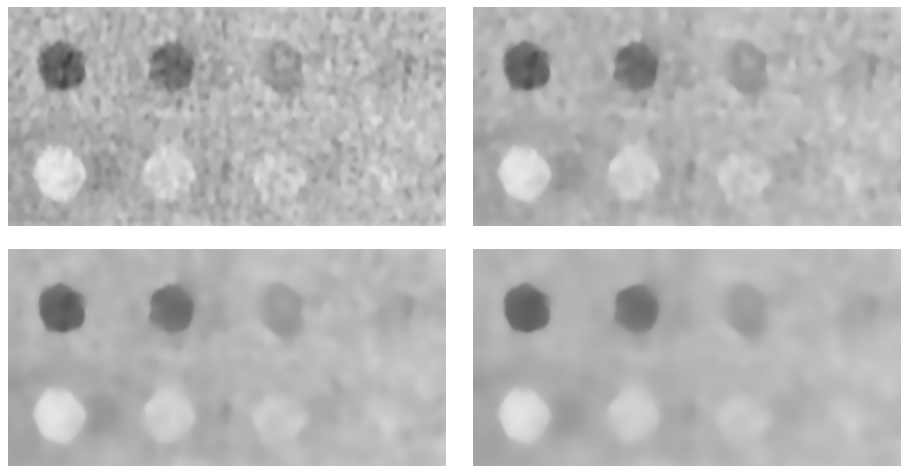
Fig. 3 Diffused images for edge enhancing diffusion $(\lambda_2 = 1)$ at time steps 1, 3, 6, and 9.

World Academy of Science, Engineering and Technology
International Journal of Medical and Health Sciences
Vol:1, No:5, 2007
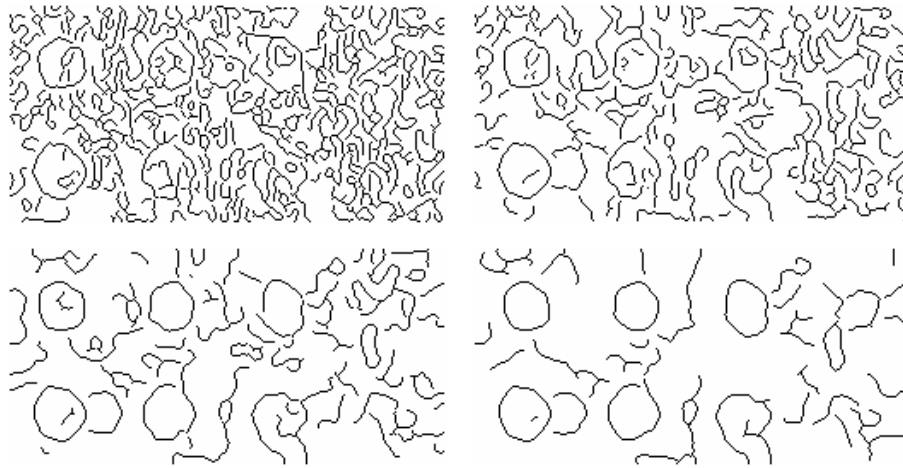
Fig. 4 Canny edge maps for Fig.3.
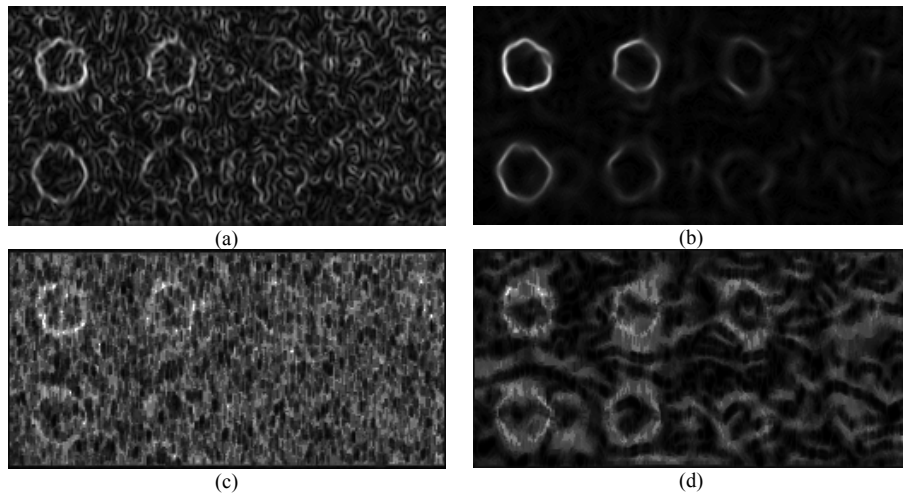
Fig. 5 Gradient maps (a,b) and scatterer density map (c,d) at time steps 1 and 9 for SDWNEED case ($\lambda_2 = 1$).
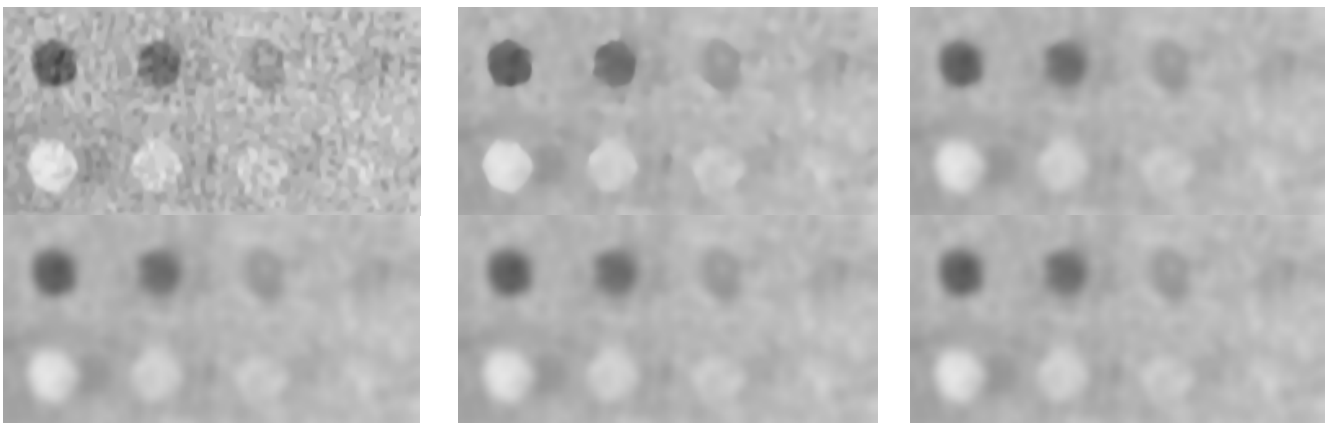
Fig. 6 Diffused images after 5 discrete time steps for K= 0.001, 0.01, 0.05, 0.1, 0.5 and 1 for SDWNEED case ($\lambda_2 = 1$).

World Academy of Science, Engineering and Technology
International Journal of Medical and Health Sciences
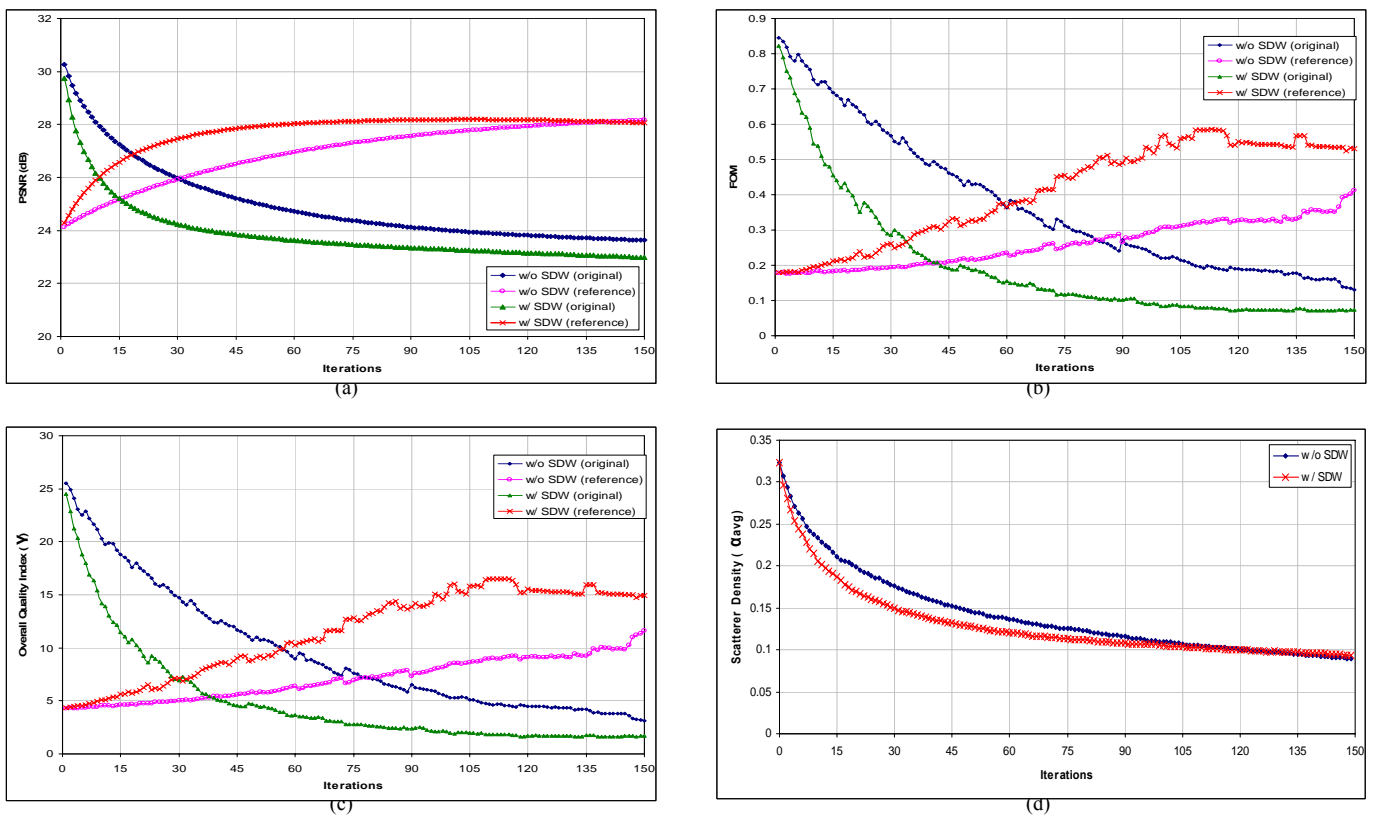Vol:1, No:5, 2007
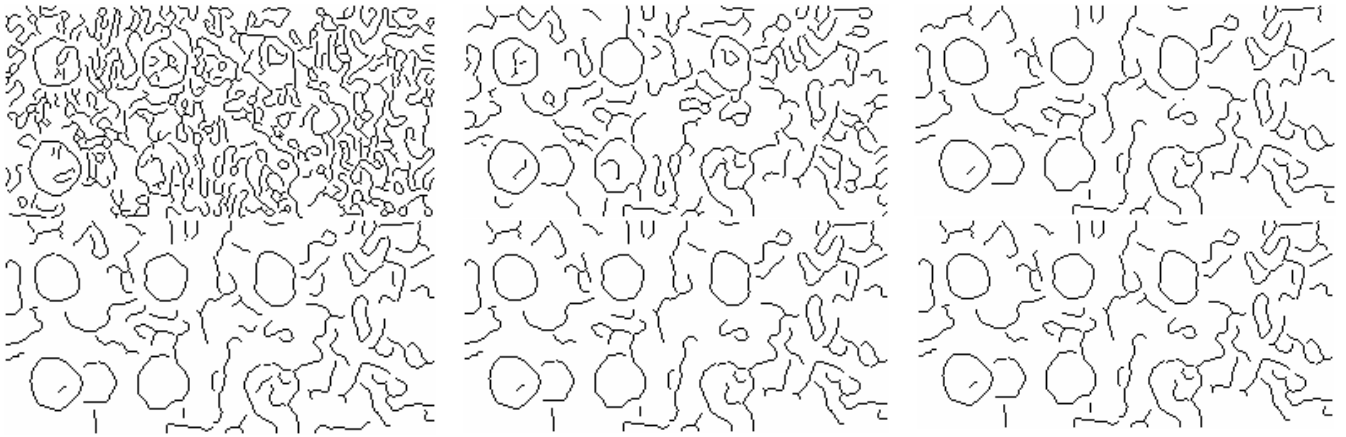
Fig. 7 Canny edge maps for Fig. 6.
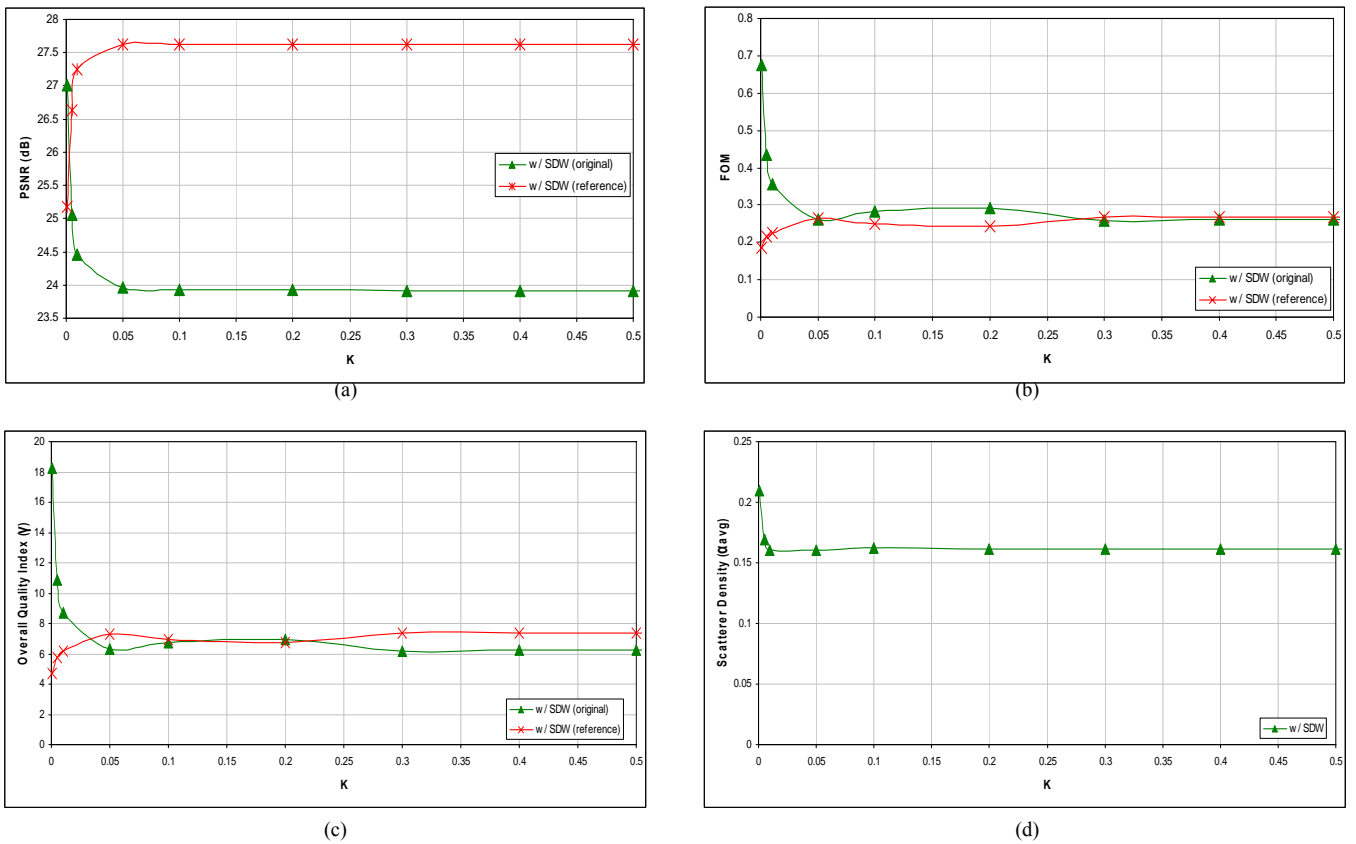
Fig. 8 PSNR (a), FOM (b), γ (c), and α_{avg} (d) of SDWNEED case ($\lambda_2 = 1$) for diffusivity functions with and without scatterer density.

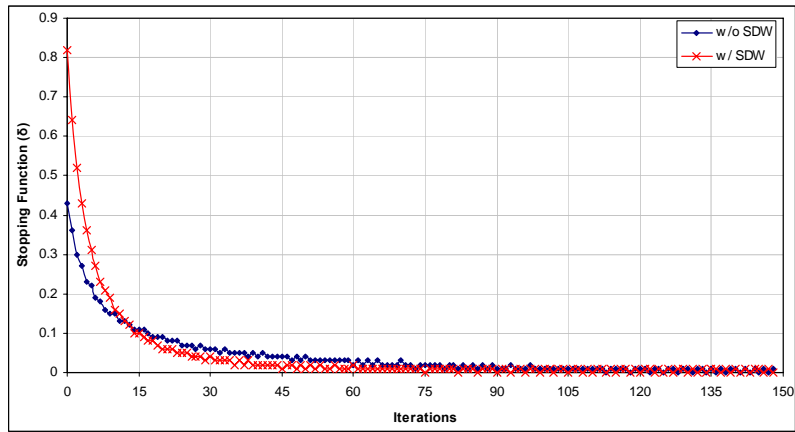World Academy of Science, Engineering and Technology
International Journal of Medical and Health Sciences
Vol:1, No:5, 2007
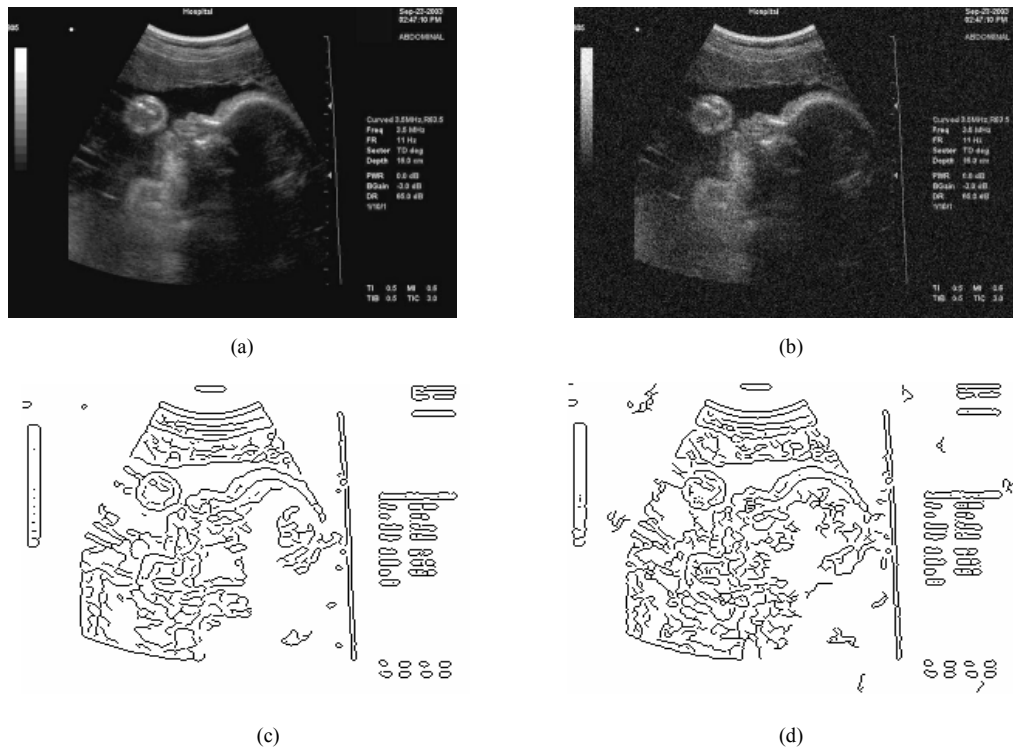
Fig. 9 Fetal face original image (a), corresponding image with additive Gaussian noise of standard deviation of 20 (b), original Canny edge map (c), Gaussian noisy Canny edge map (d).
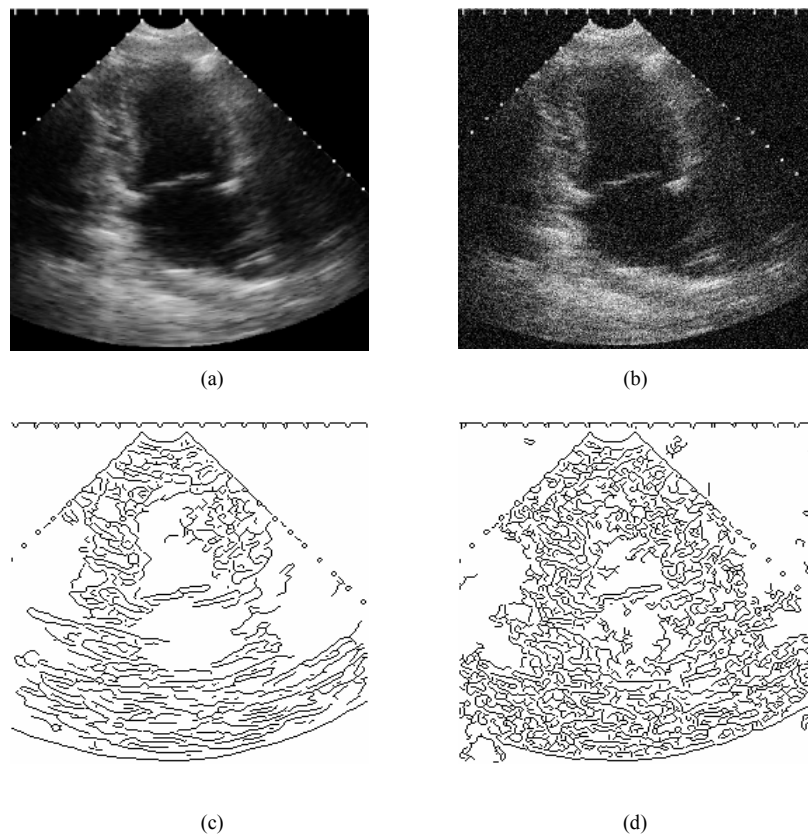
Fig. 10 Heart original image (a), its corresponding image with additive Gaussian noise of standard deviation of 20 (b), original Canny edge map (c), Gaussian noisy Canny edge map (d).

World Academy of Science, Engineering and Technology
International Journal of Medical and Health Sciences
Vol:1, No:5, 2007
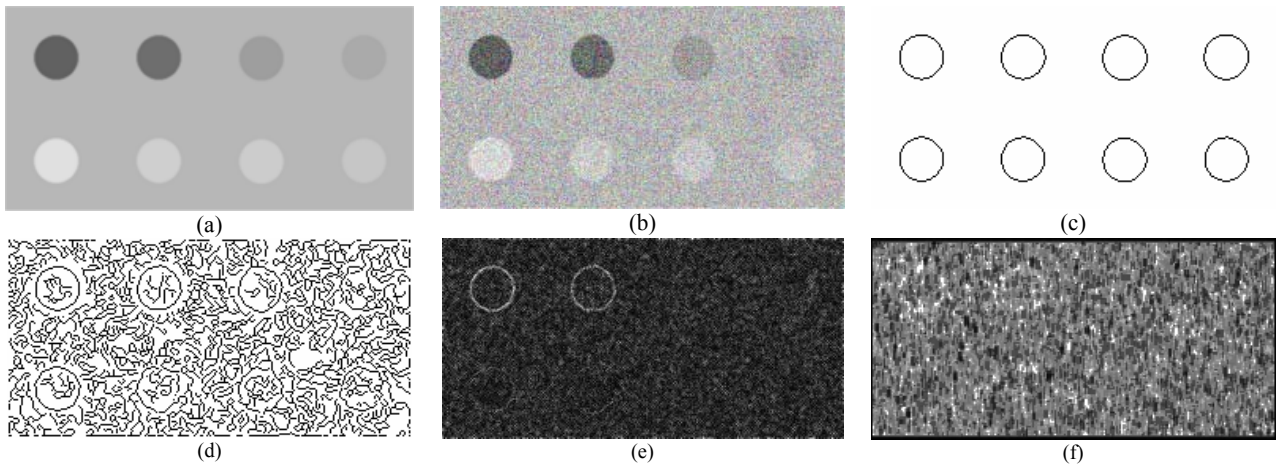
Fig. 11 Phantom reference original image (a), its corresponding image with additive Gaussian noise of standard deviation of 20 (b), original reference Canny edge map (c), Gaussian noisy Canny edge map (d), normalized noisy gradient map (e), normalized noisy scatterer density map (f).
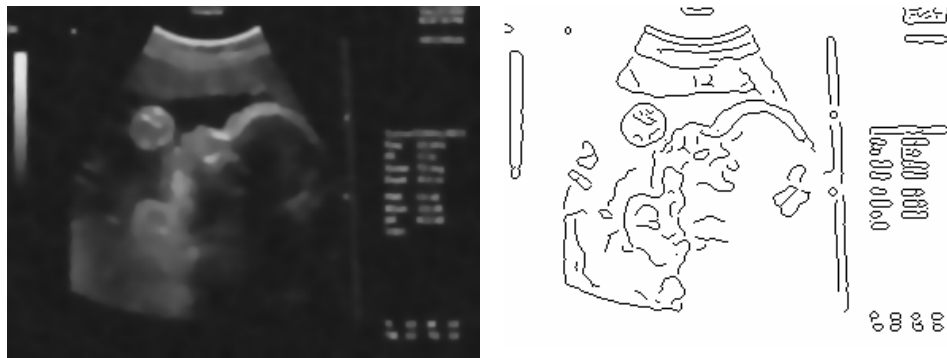
Fig. 12 Diffused fetal face image and Canny edge map for SDWNEED ($\lambda_2 = 1$).

Fig. 13 Diffused heart image and Canny edge map for SDWNEED ($\lambda_2 = 1$)

World Academy of Science, Engineering and Technology
International Journal of Medical and Health Sciences
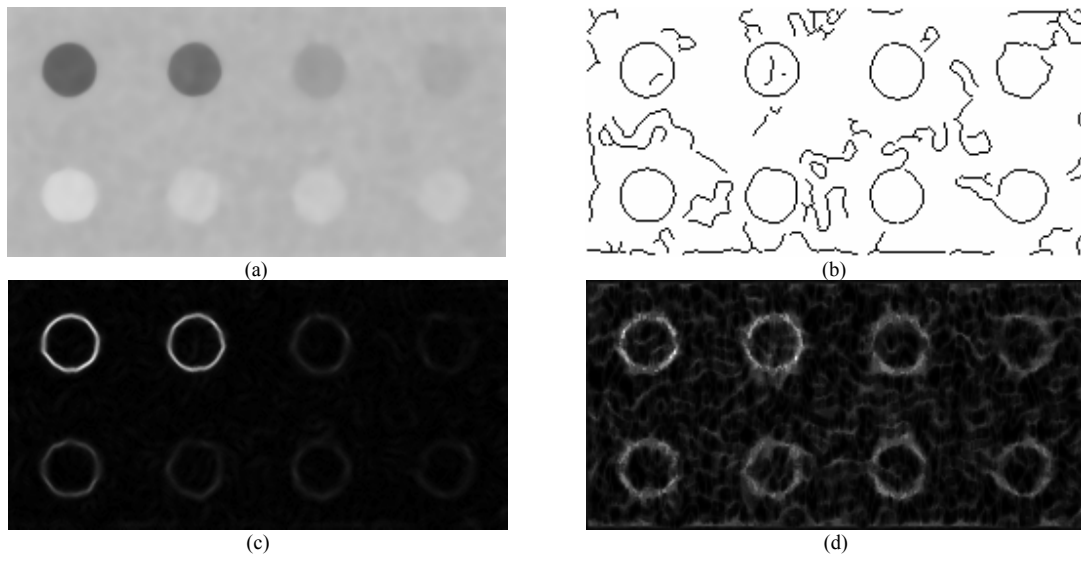Vol:1, No:5, 2007
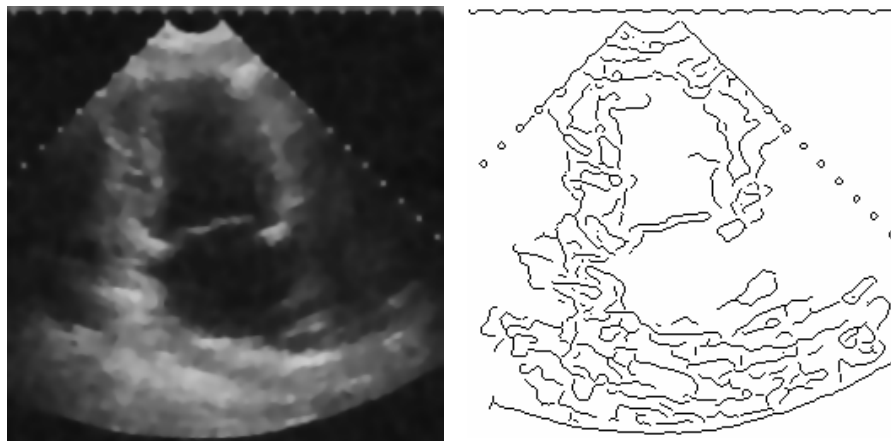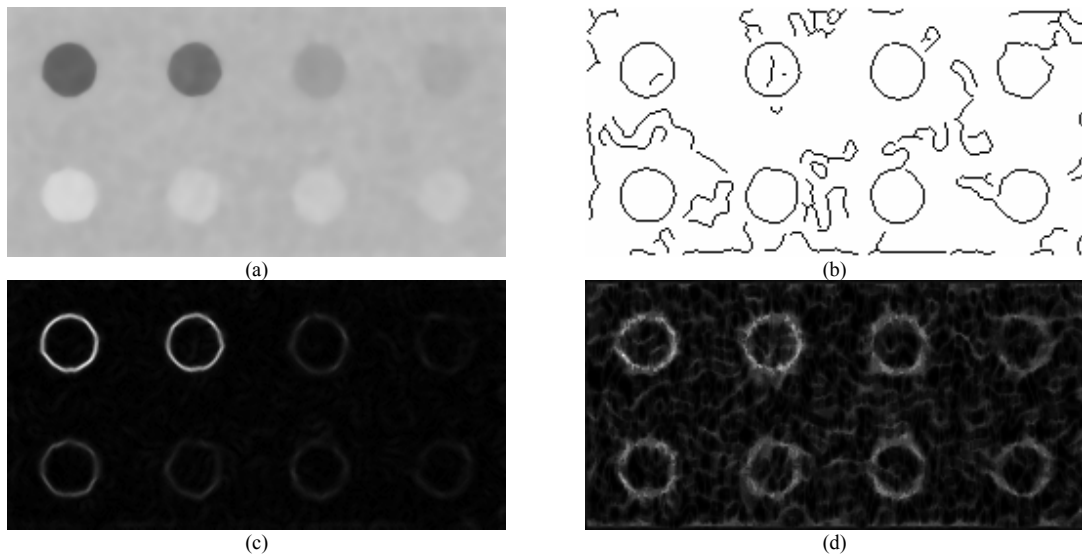
Fig. 14 Diffused reference phantom image (a), Canny edge map (b), normalized gradient map (c), and scatterer density (d) for SDWNEED ($\lambda_2 = 1$).

Fig. 15 PSNR (a), FOM (b), γ (c), and α_{avg} (d) for 150 iterations for SDWNEED case ($\lambda_2 = 1$) for diffusivity functions with and without scatterer density.

World Academy of Science, Engineering and Technology
International Journal of Medical and Health Sciences
Vol:1, No:5, 2007

Fig. 16 Stopping function for 150 iterations for SDWNEED ($\lambda_2 = 1$) for diffusivity functions with and without scatterer density.
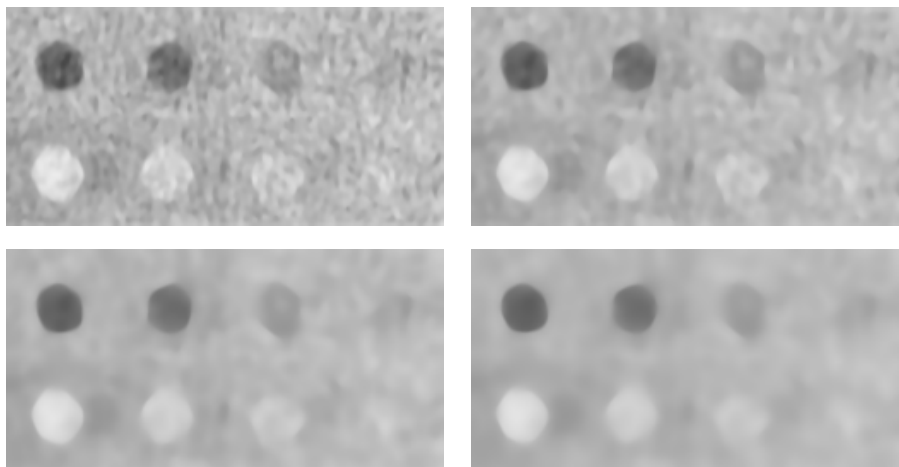
Fig. 17 Diffused image for SDWNCED at time steps 1, 3, 6 and 9.
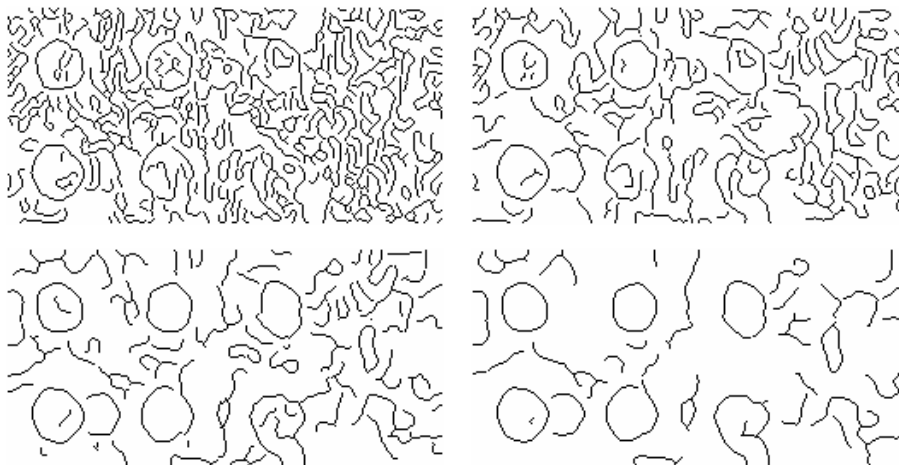
Fig. 18 Canny edge maps corresponding to Fig. 17.

World Academy of Science, Engineering and Technology
International Journal of Medical and Health Sciences
Vol:1, No:5, 2007

(a)　　　　　　　　　　　　　　　　(b)

(c)　　　　　　　　　　　　　　　　(d)
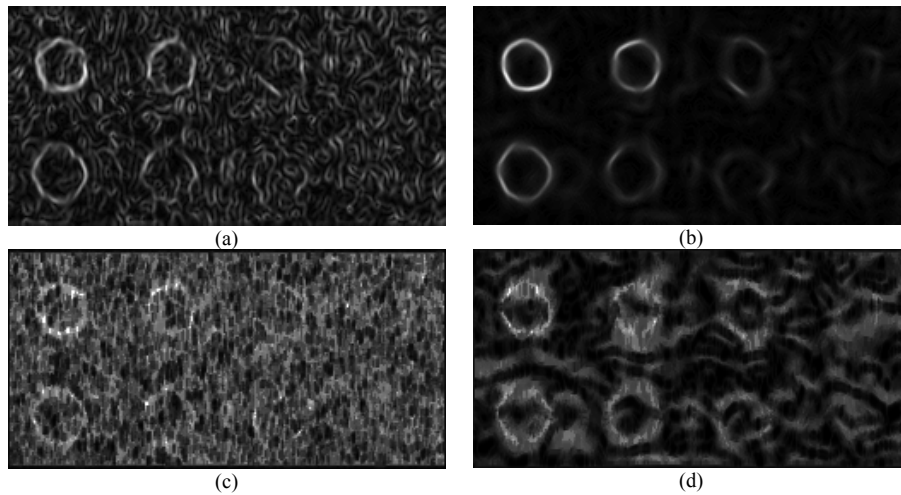
Fig. 19 Gradient maps (a,b) and Scatterer Density maps (c,d) at time steps 1 and 9 for SDWNCED.
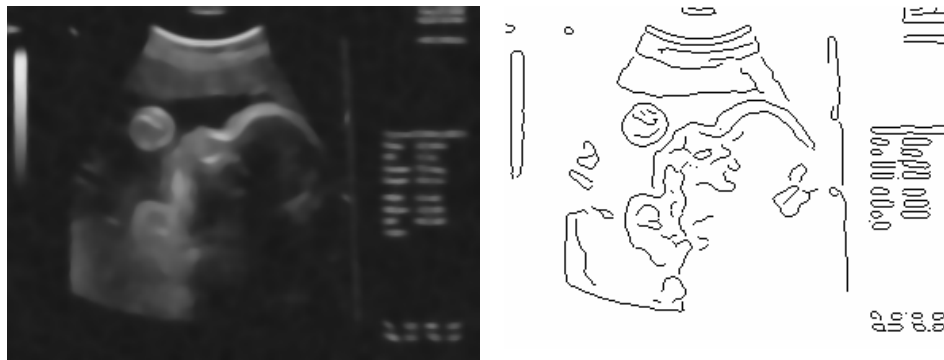
Fig. 20 Diffused fetal face image and Canny edge map for the SDWNCED.
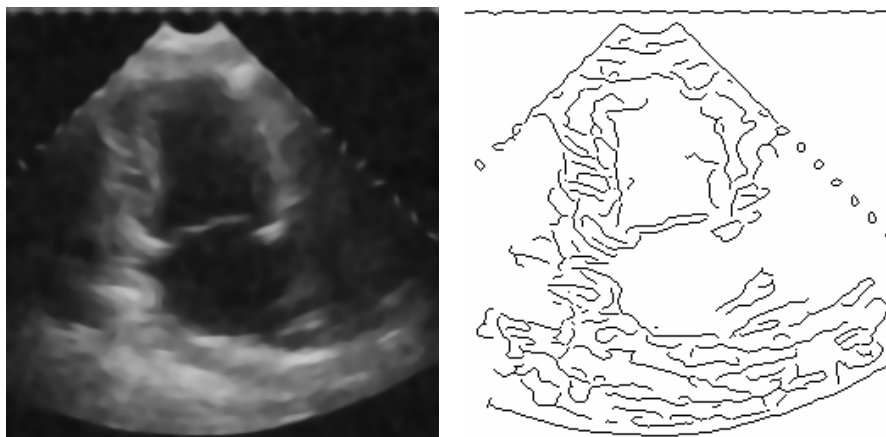
Fig. 21 Diffused heart image and Canny edge map for SDWNCED.

World Academy of Science, Engineering and Technology
International Journal of Medical and Health Sciences
Vol:1, No:5, 2007

Fig. 22 Diffused reference phantom image (a), Canny edge map (b), normalized gradient map (c), and scatterer density (d) for SDWNCED.
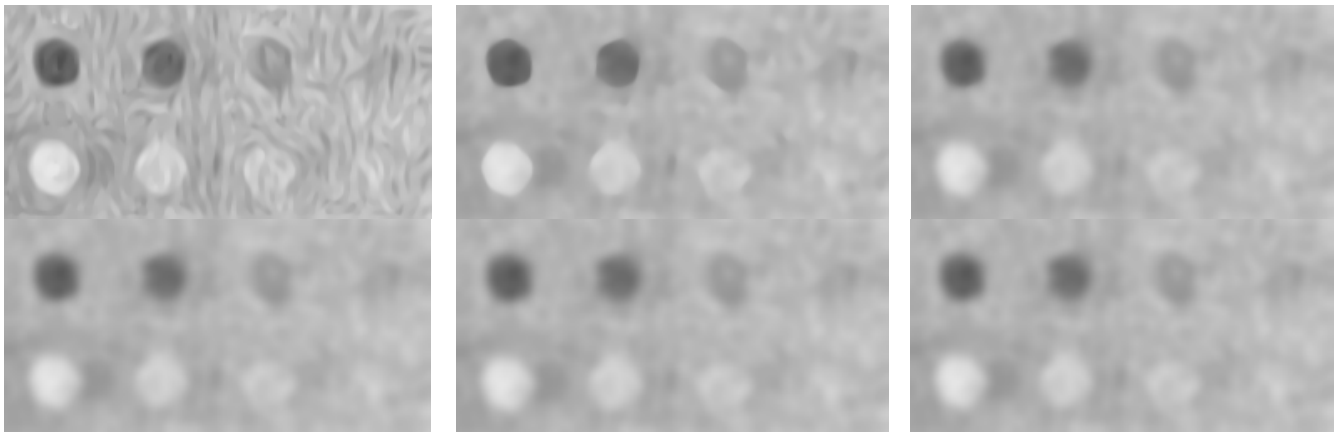
Fig. 23 Diffused images for K= 0.001, 0.01, 0.05, 0.1, 0.5, and 1.0 for SDWNCED.
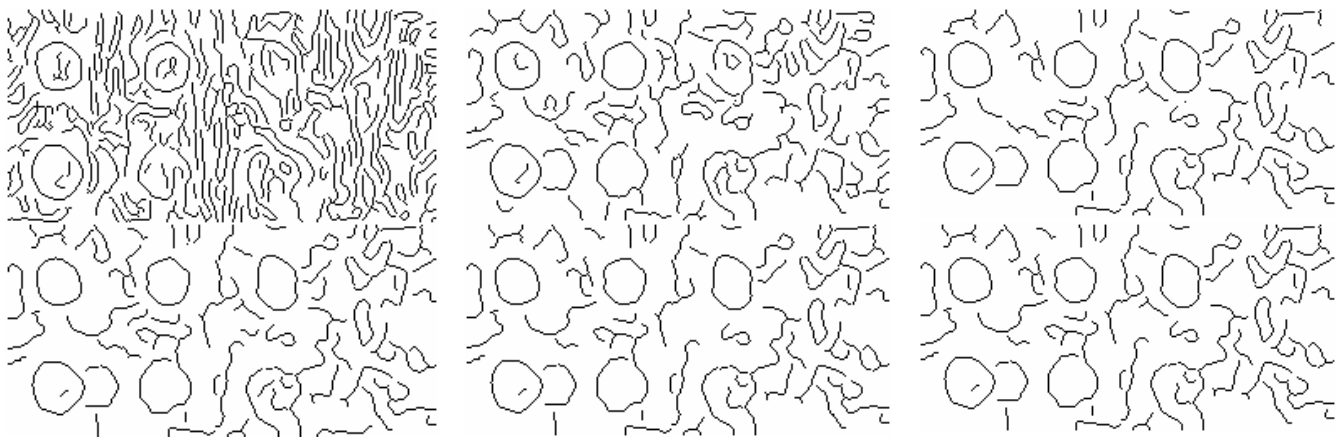
Fig. 24 Canny edge maps for Fig. 23.

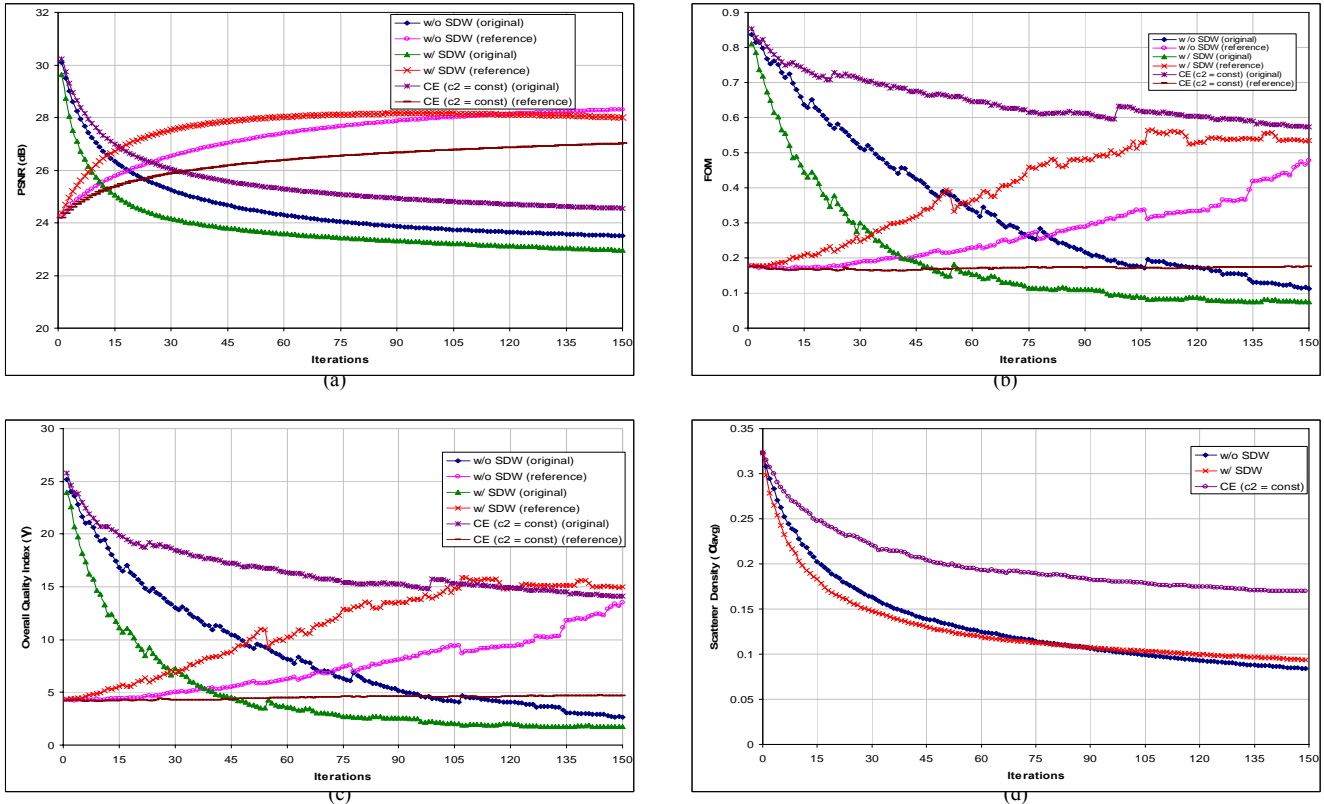World Academy of Science, Engineering and Technology
International Journal of Medical and Health Sciences
Vol:1, No:5, 2007

Fig. 25 PSNR (a), FOM (b), γ (c), and α_{avg} (d) for 150 iterations for the SDWNCED cases ($c_2 = C(x,y,t)$ and $c_2 = 0.01$).
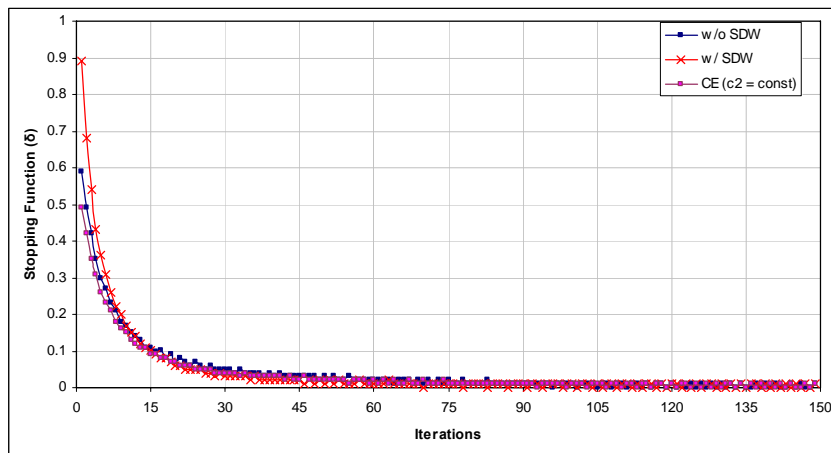

Fig. 26 Stopping function for 150 iterations for SDWNCED cases ($c_2 = C(x,y,t)$ and $c_2 = 0.01$).
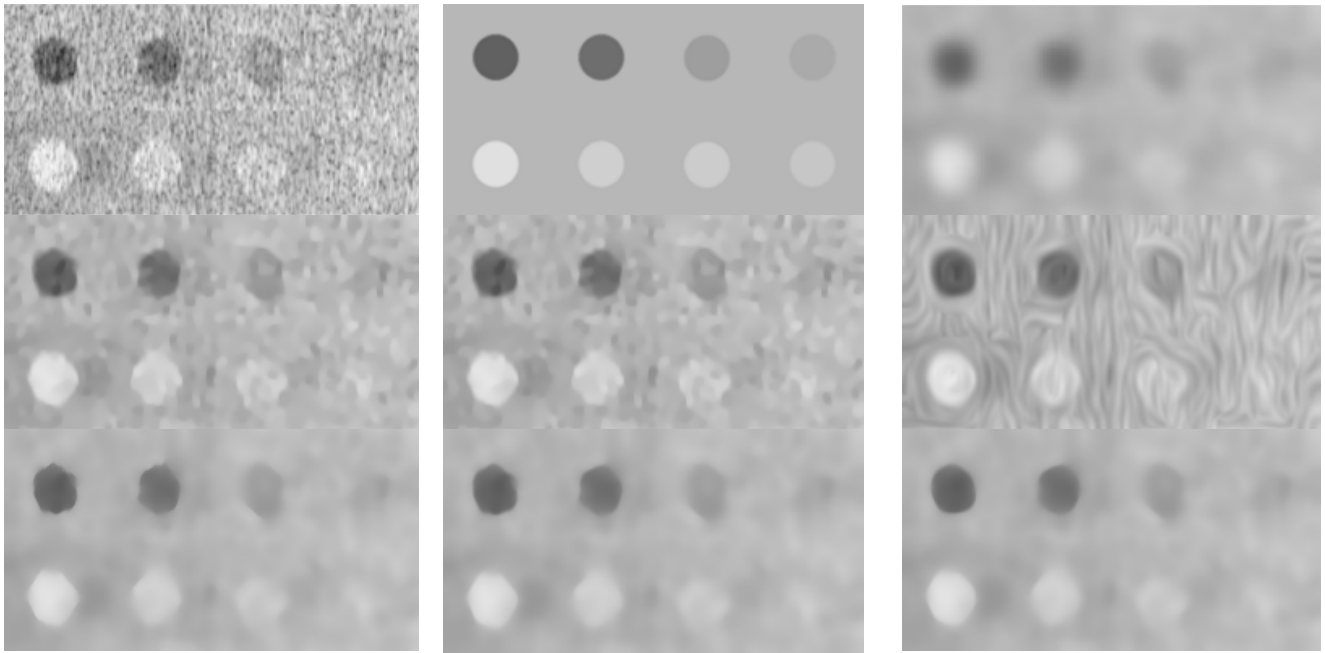
World Academy of Science, Engineering and Technology
International Journal of Medical and Health Sciences
Vol:1, No:5, 2007

Fig. 27 First row: Original phantom image, reference image, diffused image using Gaussian filter (σ=1). Second row: Diffused images using EED and CED with no scatterer density weighting, NCED ($c_2 = 0.01$). Third row: Image using SDWNEED ($\lambda_2 = C(x,y,t)/5$), SDWNEED ($\lambda_2 = 1$), SDWNCED ($c_2 = C(x,y,t)$).
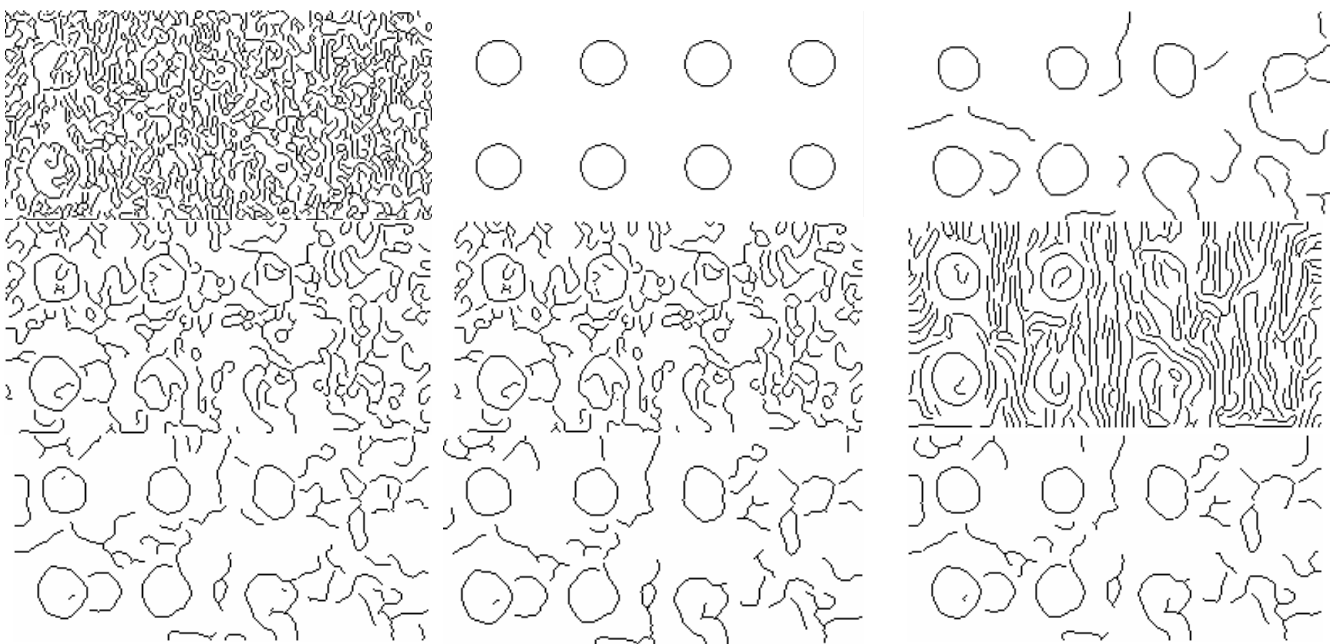

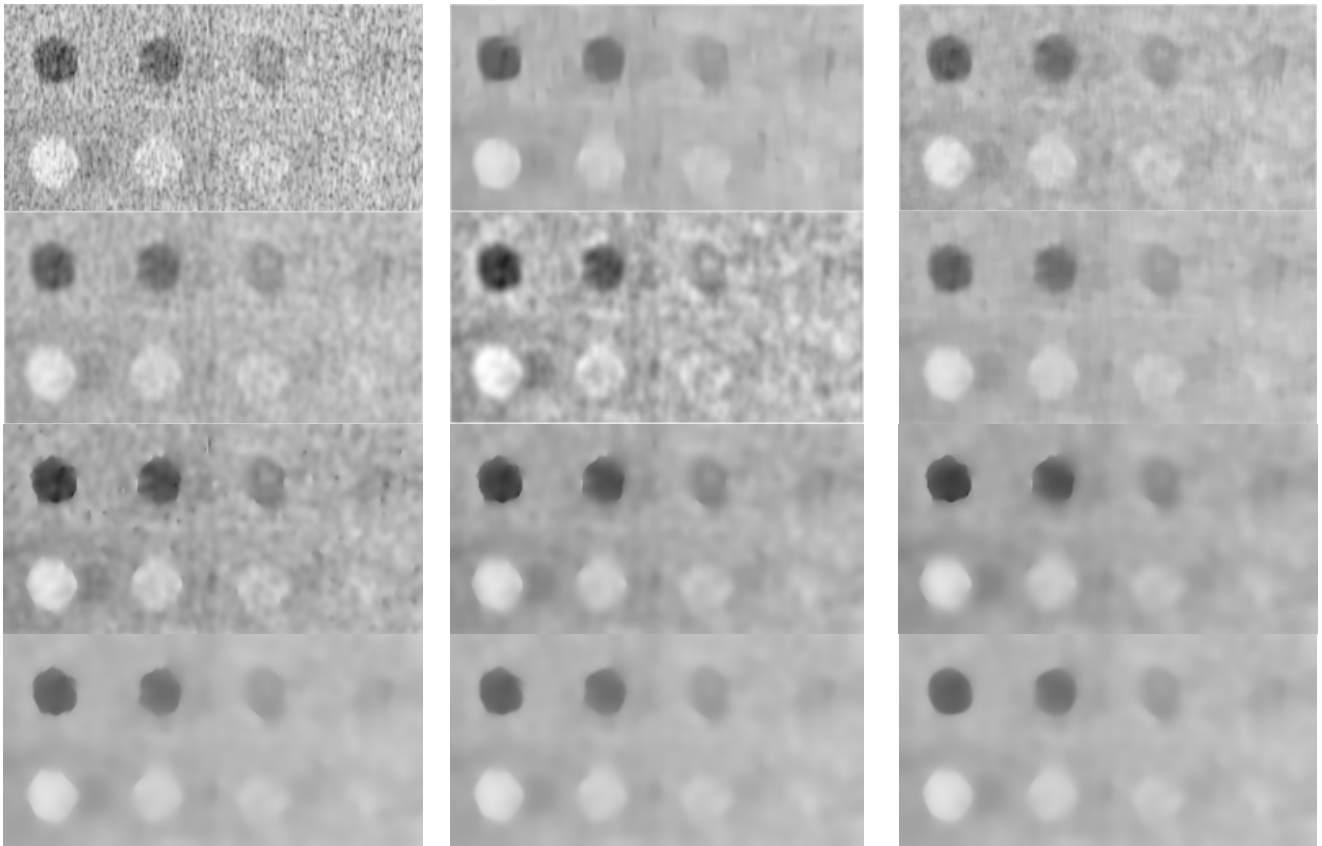Fig. 28 Canny edge maps corresponding to Fig. 27.

World Academy of Science, Engineering and Technology
International Journal of Medical and Health Sciences
Vol:1, No:5, 2007

Fig. 29 Original image, processed images with NCD, AWMF, WS, WSCE, SDWND, SRAD-45, SRAD-100, SRAD-150, SDWNEED (λ_2 = C(x,y,t)/5), SDWNEED (λ_2 = 1), and SDWNCED using proposed stopping function.
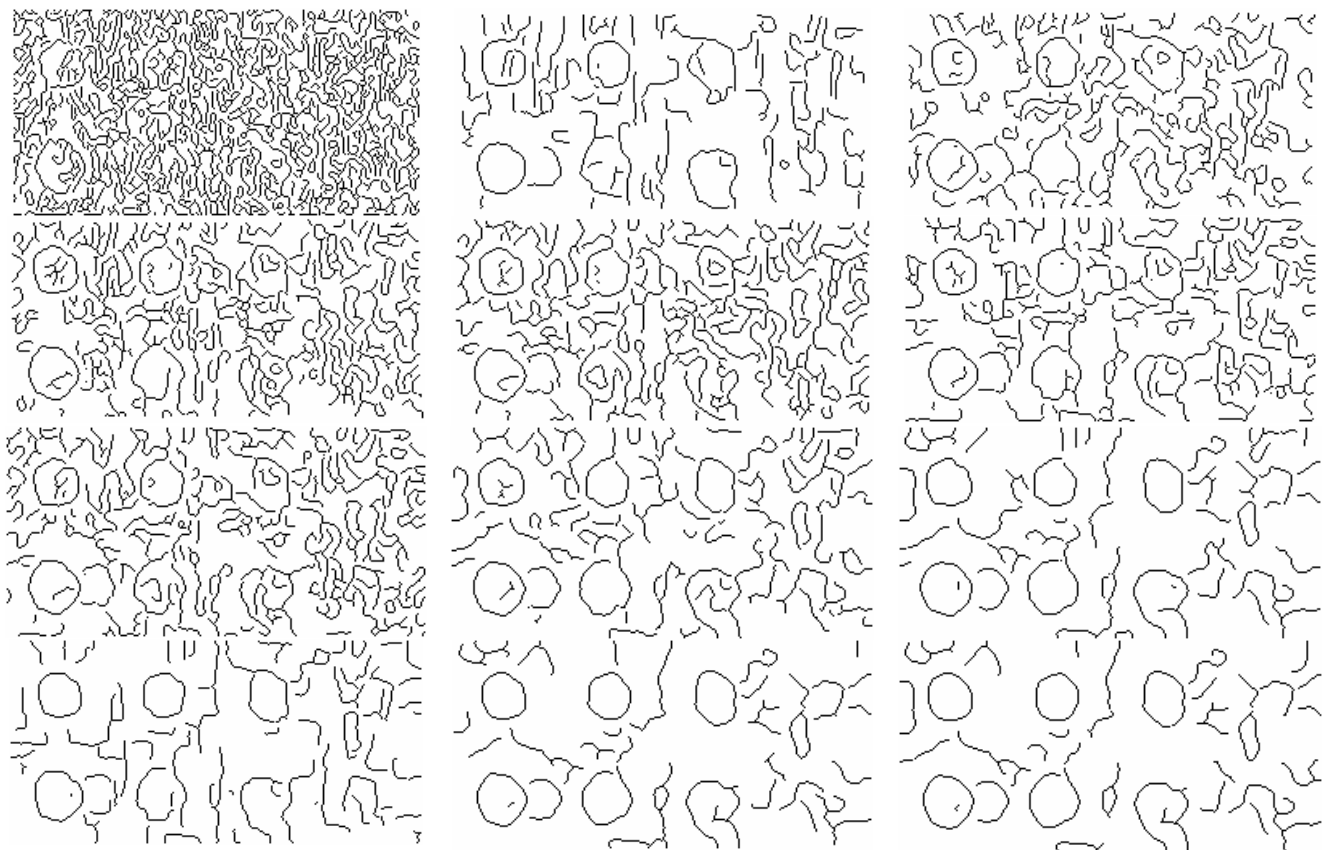

Fig. 30 Canny edge maps corresponding to Fig. 29.

World Academy of Science, Engineering and Technology
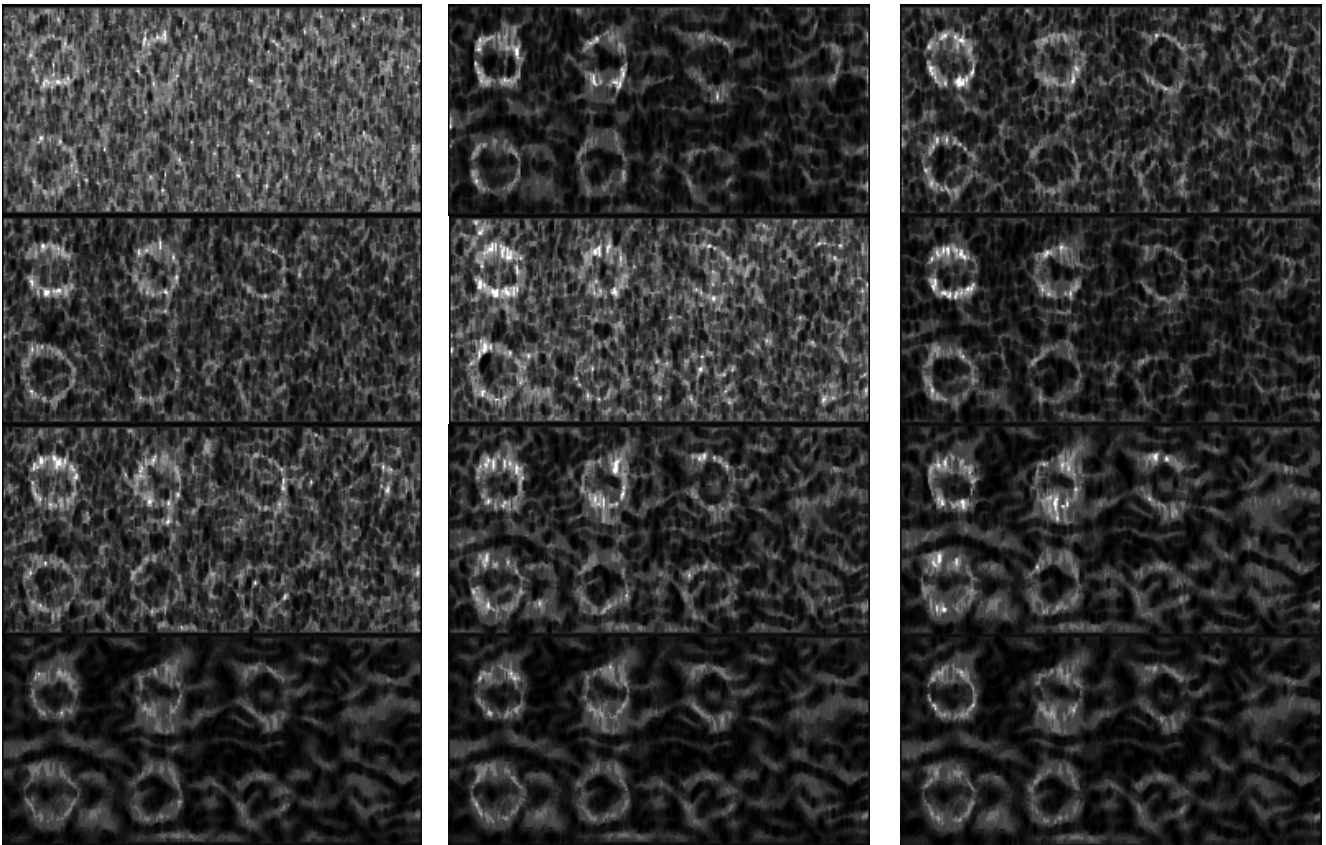International Journal of Medical and Health Sciences
Vol:1, No:5, 2007

Fig. 31 Scatterer density maps corresponding to Fig. 29.